Authors' response to referee comments

We would like to take the opportunity to thank the referees for their time, and for their valuable feedback on the manuscript. We believe that their input has helped us to improve the manuscript where possible.

Response to comments from Referee #1

General Comments

The paper presents carbon monoxide (CO) measurements in the polar upper stratosphere and mesosphere made using a new ground-based millimetre-wave radiometer (CORAM). Atmospheric observations recorded during the 2017–18 winter from Ny-Ålesund are analysed using optimal estimation retrieval techniques to determine vertical profiles of CO volume mixing ratio. The precision of the measurements is estimated and CORAM profiles are compared with overlapping CO measurements by the Aura MLS satellite instrument.

Measurements of CO in the polar middle atmosphere are important as the gas is sufficiently long-lived to be used as a tracer for characterising dynamical and transport processes associated with the winter-time polar vortex, and atmospheric wave and tide activity. The structure and extent of the polar vortex above Antarctica, and its more dynamic counterpart in the Northern hemisphere affect global circulation patterns, stratospheric ozone abundances, and atmospheric heating rates. Targeted ground-based observations of CO, such as those presented here, complement the much larger geographical coverage of satellite remote sensing datasets. The ground-based instruments provide continuous observations with the potential to resolve features occurring on short timescales.

Overall the paper is reasonably well written and presented, with adequate description of the observations, data-sets, discussion of the results, and citing of prior work. The paper covers the development, inter-comparison, and validation of an atmospheric measurement system and this fits well with the subject areas of the journal. My main criticism is the lack of important details about the CORAM instrument itself. The main novelty in the work is the new design of this radiometer that incorporates optical/electronic components. The authors suggest that this design improves the performance/cost over previous heterodyne radiometers used for this type of measurement. As indicated in my specific comments below, the sections (2.1 and Figure 1) of the paper describing the new instrument need expanding with further technical details.

The manuscript would benefit from a more thorough description of existing CO measurement systems including those utilising the thermal IR bands of CO to make middle atmosphere observations. The conclusions section should include clear statements as to how well the anticipated improvements in performance were achieved. I've also identified a number of areas in the text and figures where clarifications are needed and the presentation could be improved. I recommend that the authors address all of these points before the revised paper is considered for publication in Atmospheric Measurement Techniques.

Specific Comments

Title

Lines 1–2. It's unclear what the measurement technique is from the title. Perhaps the words 'microwave (or, millimetre-wave) radiometer' could be included in the title?

The title has been changed to read:

"Ground-based millimetre-wave measurements of middle-atmospheric carbon monoxide above Ny Ålesund (78.9°N, 11.9° E)."

2.1 CORAM and Figure 1

The technical description of the new instrument is difficult to follow and lacks important details about the novel electronic/optical components. Figure 1 is an unclear, poor quality diagram. It may be better to have two instrument diagrams, one showing the optical layout including the atmospheric and calibration load beam paths, and the other showing the electronic signal chain.

Figure 1 has been remade for clarity and now includes a simplified version of the quasioptical system showing the relevant components. The caption of Figure 1 has been edited to reflect the changes. Combined with the expanded information in Section 2.1, the reader has a concise view of the instrument.

"After the pointing mirror, the atmospheric signal is directed by a series of quasioptical components through a window in a cryocooler and fed into a corrugated horn antenna. The signal is amplified by a 230 GHz LNA. The unwanted sideband at ~ 213.5 GHz is supressed with a waveguide filter before the signal is mixed with the local oscillator (LO) signal (111 GHz) using a sub-harmonic mixer. Now at an intermediate frequency of 8.5 GHz, the signal exits the cooler and is amplified with another LNA before being further

downconverted to 0.5 GHz and analysed by a Fast Fourier Transform Spectrometer (FFTS). Figure 1 shows a schematic drawing of the receiver including the components in the cryocooler, as well as a simplified version of the quasioptical layout. The cryocooler makes use of a CTI Cryogenics 350 CP coldhead and a CTI Cryogenics 8200 compressor, as well as a helium cooling machine."

"Fig 1: Schematic of the CORAM receiver and simplified quasioptics. A rotatable mirror selects a signal from either the atmosphere, warm target, or cold target. The signal is directed by a parabolic mirror to a path length modulator that comprises a polarising wire grid, an absorber, and an oscillating rooftop mirror. The signal passes through a window in the cryocooler where it is directed to the receiver with an elliptical mirror. The signal enters the corrugated feed horn and encounters the RF LNA, a waveguide filter (BPF), and a sub-harmonic mixer (SHM). At the SHM the signal is downconverted to an intermediate frequency (IF) of 8.5 GHz. The IF signal exits the cryocooler and passes through a room temperature LNA. The RF (atmospheric) signal is mixed at the SHM with a local oscillator (LO), which is an 18.5 GHz signal from a phase-locked dielectric resonator oscillator (PDRO) that is passed through a x6 frequency multiplier, to provide 111 GHz. The IF out signal will be further downconverted to 0.5 GHz before being analysed by the Fast Fourier Transform Spectrometer (not shown here). Further details on quasioptical components can be found in Goldsmith (1998)."

For the atmospheric view, why was a 20° elevation chosen and what is the azimuthal angle?

Motivation for the choice of viewing angle is now included in Section 2.1. The number is actually 21 degrees and the azimuth is 113 degrees:

"The atmospheric signal enters the lab through a window that is transparent to millimetre-wave frequencies, and meets the pointing mirror of CORAM, angled at 21° elevation. This angle was chosen by performing a series of atmospheric radiative transfer simulations at different elevation angles, using a climatological polar winter atmosphere, and determining which angle provided the strongest CO spectral line. The choice of angle is a trade-off of maximum path length through the target gas in the atmosphere, and minimum attenuation of the target signal by atmospheric water vapour that is primarily in the troposphere. The azimuth angle of the atmospheric signal is 113°, defined by the lab in which CORAM is held."

What is the field-of-view of the instrument and how far away from the instrument is the observed region of the middle atmosphere?
The HPBW is now included in Section 2.1.
"The quasioptical setup has an antenna pattern with a half-power-beam-width of ~ 5°."

With an elevation angle of 21 degrees, the distance from the instrument can be calculated at any altitude. The distance at 60 km is now included in Section 3.1.
"MLS measurements are subset to within ±2° latitude and ±10° longitude of CORAM, calculated at 60 km altitude along the line of sight of CORAM (~ 156 km horizontally from the lab)."

What type of cryocooler is used?
Section 2.1 now contains the following information:

"The cryocooler makes use of a CTI Cryogenics 350 CP coldhead and a CTI Cryogenics 8200 compressor, as well as a helium cooling machine."

How much improvement in SNR is achieved by amplifying the 230 GHz signal by the first-stage LNA, rather than amplification occurring after down conversion to a lower frequency?
Information is now included that describes an estimate of the difference in the receiver temperature when switching the position of the LNA relative to the mixer, as well as an outline of the radiometer equation, which describes how the SNR is related to the system temperature. The system temperature includes more contributions than just the receiver temperature of CORAM, which is mainly from the LNA/filter/mixer. The SNR is not a fixed value and will change depending on the atmospheric conditions. This information is now clarified in Section 2.1.

"An estimate of the improvement in the receiver temperature (Janssen, 1993) can be made using a noise temperature cascade analysis. A variation of Friis' equation (Vowinkel, 1988) for two components in succession is $T = T_1 + T_2/G_1$, where T_1, and T_2 are the respective noise temperatures of the first and second components, G_1 is the linear gain of the first component, and T is the total noise temperature. The noise temperature of the LNA plus waveguide filter was measured to be 1350 K at room temperature, and the linear gain was measured at 158 (corresponding to 22 dB) (Fig. 2b). The noise temperature of the sub-harmonic mixer is ~1500 K at room temperature and has a linear gain of ~0.16

(corresponding to -8 dB). Applying Friis' equation with the LNA preceding the mixer gives a noise temperature of ~1360 K. The same calculation with the mixer as the first component gives a noise temperature of ~9800 K. The dominant contribution to the receiver temperature of CORAM is from the LNA/filter/mixer. Cooling the components can considerably reduce their noise temperature. Figure 2b shows the noise temperature and gain of the LNA + filter, measured at room temperature. Figure 2c shows the receiver temperature for CORAM measured at the exit of the cryocooler, with the cryocooler components at a typical temperature of 39 K. At 8.5 GHz, the receiver temperature is below 350 K.

The system temperature, $T_{sys,}$ includes contributions the second downconversion, the atmospheric background and signal, and quasioptical spillover (Parrish et al., 1988, Janssen, 1993, Stanimirović et al., 2002). The system temperature is related to the measurement time through the so-called ideal radiometer equation: $\sigma_T = T_{sys} / (Bt)^{1/2}$, where σ_T is the statistical noise on a measured spectrum, B is the frequency bandwidth of the measurement, and t is the integration time for the measurement. This relationship determines the measurement time required to provide a given SNR. The single sideband T_{sys} for CORAM is ~600 K. The atmospheric measurements are all made with the same elevation angle and so the individually recorded spectra can be averaged together to reduce the SNR. The measurements used here have been spectrally averaged over approximately 1 hour, including time used to calibrate the signal. Finer time resolutions that still yield usefully high SNRs are possible. Since T_{sys}, as defined here, contains a component from the atmospheric background, the SNR of a given measurement will vary with the atmospheric conditions at the time, with a more opaque troposphere giving rise to a smaller SNR. An ad-hoc indication of "bad" weather conditions was found to be a measurement with a baseline temperature > 230 K, and these measurements were discarded."

Has this type of direct amplification been used before?

This configuration has been used for other radiometers that operate at lower frequencies. The following information has been included in Section 2.1. The new citations have been included in the reference list.

"This configuration has been used before for similar instruments e.g. MIAWARA-C (Straub et al. 2010) and GROMOS-C (Fernandez et al., 2015), which measure ozone at 110 GHz, and water vapour at 22 GHz, respectively."

For the FFTS, what alias is used, what is the frequency resolution, and why is this high spectral resolution needed?

With a bandwidth of 1 GHz and 16384 channels the FFTS provides a frequency resolution of about 61 kHz. A higher frequency resolution, depending on the Doppler width, is required for resolving the mesospheric part of the spectrum. The following text is now included in Section 2.1

"The FFTS is an Acqiris AC240 and has a bandwidth of 1 GHz with 16384 channels, providing ~61 kHz resolution. A high spectral resolution, depending on the Doppler width of a spectral line (~300 kHz in this case), is required for resolving the mesospheric contribution to the spectrum. CORAM performs the Fourier Transform in real time and the fully resolved spectrum is stored."

It is not clear what is meant by "what alias is used?".

What baseline SNR is achieved in the recorded spectra?

The SNR of a particular measurement is governed by the system temperature, which includes an atmospheric component. The weather is quite variable at Ny Alesund, and this changes the SNR from measurement to measurement. The equation that describes the relationship between the SNR and the system temperature is now given in Section 2.1.

"The system temperature, $T_{sys,}$ includes contributions from the second downconversion, the atmospheric background and signal, and quasioptical spillover (Parrish et al., 1988, Janssen, 1993, Stanimirović et al., 2002). The system temperature is related to the measurement time through the so-called radiometer equation: $\sigma_T = T_{sys} / (Bt)^{1/2}$, where σ_T is the statistical noise on a measured spectrum, B is the frequency bandwidth of the measurement, and t is the integration time for the measurement. This relationship determines the measurement time required to provide a given SNR. The single sideband T_{sys} for CORAM is ~600 K. …… . Since T_{sys}, as defined here, contains a component from the atmospheric background, the SNR of a given measurement will vary with the atmospheric conditions at the time, with a more opaque troposphere giving rise to a smaller SNR. An ad-hoc indication of "bad" weather conditions was found to be a measurement with a baseline temperature > 230 K, and these measurements were discarded."

What are the integration times for the calibration and atmospheric signal measurements?

CORAM currently measures each target with equal integration times. An error propagation of the total power formula shows, that the noise on the calculated spectrum depends on the time the calibration blackbodies are measured and on the level the target signal (here: the atmosphere) has. As a compromise, equal measuring times for all sources have been

chosen. The data used here has been spectrally averaged over a 1 hour period including time for calibration.

Section 2.1
"The measured atmospheric signal is calibrated using two blackbody targets at known temperatures (measured with mounted sensors): a cold target in the cryocooler at ~ 70 K and a warm target at ~ 293 K. The integration times for each blackbody is the same as that for the atmospheric signal."

"The measurements used here have been spectrally averaged over approximately 1 hour, including time used to calibrate the signal."

Is the instrument located outdoors or inside a building and, if the latter, what external window material was used to transmit the atmospheric signal?
The instrument is located inside a lab and the atmospheric signal enters through a foam window that is transparent to millimetre-wave frequencies. This information is now included in Section 2.1. Investigation of possible attenuation of the atmospheric signal by the window has been included in Section 5: Conclusions and future work.

Section 2.1
"The atmospheric signal enters the lab through a window that is transparent to millimetre-wave frequencies, and meets the pointing mirror of CORAM, angled at 21° elevation."

Section 5
"Future work with CORAM will include: Integration of a new local oscillator due to a failure of the original, and investigation of possible attenuation of the atmospheric signal by the laboratory foam window."

What effects do local weather conditions have on the ground-based observations?
Local weather conditions can cause some measurements to be unusable. An ad-hoc indication of "bad" weather conditions was found to be a measurement with a baseline temperature > 230 K, and these measurements were discarded. This information is now included at the end of Section 2.1.

Technical Corrections

Abstract

Page 1, line 10. 'CO emissions'. It should be clarified that this refers to CO microwave (or, millimetre-wave) line emissions rather than, e.g. CO emissions from wildfires or industrial production.

The line has been edited to read *"… spectral emissions …"*

Page 1, line 16. The exact start and end dates of the new dataset should be given.

This has been added.

1. Introduction

Page 1, lines 18–23. The authors should make it clear whether they are referring just to microwave (or, millimetre-wave) radiometers or also to other instruments operating at long-wave frequencies to measure thermal emissions from atmospheric molecules. If by 'electronic manipulation' the authors mean the use of heterodyne techniques then that should be clearly stated. Similarly, if 'reliance on the sun' is referring to solar absorption / occultation measurements then that should be made clear.

The wording has been changed to include "milimetre-wave" and refer to solar absorption measurements. The latter part has been expanded to clarify the benefits of this type of instrumentation, including a reference to coherent detection with heterodyne receivers. A citation for Jannsen (1993), has been added for further reading.

"Millimetre-wave (also referred to as microwave) radiometers are powerful tools for measuring the composition of the atmosphere. This is particularly true for areas where there are prolonged night-time periods, such as the poles. The instruments can measure emissions from molecules in the atmosphere, in contrast to solar absorption measurements that rely on the sun. Coherent detection of the atmospheric signal, achieved through heterodyne receivers, and electronic manipulation of that signal, make it possible to detect and resolve spectral lines with very low intensities, especially when the electronics are cooled to low temperatures, thus producing lower thermal noise (Janssen, 1993)."

Page 1, line 26. 'An example of this…' An example of what?

The sentence has been changed to the following:

"During polar night, CO concentrations increase in the middle atmosphere due to the vertical branch of the residual mean circulation bringing CO-rich air from higher altitudes (Smith et al., 2011; Garcia et al., 2014)."

Page 1, line 30. 'allows for more CO-poor air…' should probably be changed to 'allows more CO-poor air…'
This has been changed.

Page 2, line 14. 'on smaller timescales…' Smaller than what?
The sentence directly before this one refers to variation in VMR on a timescale of days: *"+450 m/day'.* The next sentence (the one in question) refers to variations on timescales smaller than this, explicitly stated as *"minutes to hours"*.

Page 2, line 14. What type of waves are being referred to here?
No distinction is made here. The five references offer analyses on the types of waves that cause disturbances on these time scales.

Page 2, lines 16–17. 'relatively high time resolution'. Relative to what?
The sentence has been edited to read:

"Data from ground-based radiometers with high time resolution (order of an hour or less) have be used to investigate small periodic fluctuations in ozone (O_3) and water vapour (Hocke et al., 2006; Moreira et al., 2018, Schranz et al., 2018)."

Page 2, lines 19–21. A time resolution of ≤1 hr may make the technique well-suited to observe periodic fluctuations in CO. However, the authors should consider how the limited resolution in vertical and horizontal directions would impact on observing structures on varying spatial scales associated with gravity waves, other dynamical processes, and the vortex edge.
This future work will most likely be performed using techniques, or variations thereof, that have been used in the cited literature. The measurements in these citations come from both ground-based and satellite-borne instruments with varying degrees of spatial resolution. As such, the paragraph in the manuscript has been edited to include the following:

"As with the ground-based and satellite-borne instruments in the works cited above, the analyses must be performed within the context of the limited spatial resolution of the measurements."

Page 2, line 24. The authors should justify why the measurements provide a 'needed increase in Arctic coverage and an excellent opportunity…' How well placed are the Kiruna and Ny-Ålesund instruments for observations near the vortex edge and inside the winter-time Arctic polar vortex?

Information has been added on the sparsity of recent polar datasets to justify the need for more.

"CO profiles from satellite measurements have been used regularly to study processes in the polar winter atmosphere (e.g. Damiani et al., 2014; Lee et al., 2011; Manney et al., 2009; McLandress et al., 2013), but recent ground-based CO datasets in the polar (and nearby) regions have been sparse: The Onsala Space Observatory instrument (57°N, 12°E) (Forkmann et al., 2012), which produced data for 2002 – 2008, and from 2014; The ground-based millimetre-wave spectrometer (GBMS) at Thule Air Base (76.5°N, 68.7° W), used to investigate the Arctic winter of 2001/2002 (Muscari et al., 2007) and the sudden stratospheric warming (SSW) in 2009 (Di Biagio et al., 2010); The British Antarctic Survey (BAS) radiometer data at Troll Station (72°S, 2.5°E) covers February 2008 to January 2010 (Straub et al., 2013). These instruments also measure the rotational transitions of CO and can operate during polar night."

The vortex is not a stable structure in space, but having two instruments operating at the same time that are 12 degrees apart within the polar region will provide opportunities to measure inside/outside/in the edge of the polar vortex.

Page 2, line 25. A reference should be given to sudden stratospheric warmings.

Sudden stratospheric warmings are now mentioned earlier, in Section 1, in relation to the citation of Di Biagio et al. (2010).

2. Instrument and measured data

2.1 CORAM

Page 3, line 4. Define 'AWIPEV'.

AWIPEV is the name of the research base.

2.2 Inversion method

Page 4, line 7. Define 'WACCM4'.

This is now defined as the Whole Atmosphere Community Climate Model.

Page 4, line 7. Presumably data at the WACCM4 grid-point closest to the CORAM observations are used?
A line is added directly after to clarify:

"Model output for the grid point encompassing Ny-Ålesund is used."

Page 4, line 8. '132-layer grid between approximately ground and 130 km altitude'. Why is this a 132-layer (altitude) grid rather than 131 layers (i.e., 0–1 km, 1–2 km, …, 130–131 km)?
The grid is in pressure space. It does not follow altitude in such a fashion. The sentence has been edited to clarify that the grid is in pressure space:

"The output is on a 132-layer pressure grid between approximately ground and 130 km altitude."

Page 4, line 12. 'CO emissions are attenuated by water vapour in the atmosphere'. It should be clarified that attenuation is due to water vapour absorption of the CO signal. Presumably most of the water vapour is in the troposphere?
The sentence has been edited to clarify:

"CO emissions are attenuated by absorption due to water vapour in the atmosphere (mostly in the troposphere) and this is accounted for by including the water vapour continuum by Rosenkranz (1998) in the forward model and inversion."

Page 4, line 14. 'O3 spectral line lies at 231.28 GHz…' The O3 line position (i.e. line centre) is at 231.28 GHz.
The sentence has been edited to clarify that the centre of the spectral line is at 231.28 GHz.

"O_3 is also simultaneously retrieved with CO, as an O_3 spectral line is centred at 231.28 GHz."

Page 4, line 15. 'The spectroscopic line data used here is from…' should be changed to 'The spectroscopic line data used here are from…'
This has been fixed.

Page 4, line 22. 'ECMWF information is available four times per day'. Rephrase to remove any ambiguity, i.e. to make it clear that the ECMWF data are at six hour intervals.

This is now clarified.

"ECMWF information is available daily at 6-hour intervals, beginning at midnight, and covers up to 0.01 hPa altitude"

Page 4, line 23. Change 'The temperature data is smoothed…' to 'The temperature data are smoothed…'
This has been fixed.

Page 4, lines 30–31. Suggest shorten 'Three primary sinusoids were found to be present, …' to 'Three primary sinusoids were found …'
Agreed. This has been changed.

Page 4, line 32. 'large compared with the width of the CO spectral line'. What is the width of the CO spectral line?
This information has been added to the line.

"The periods of the sinewaves are large compared with the width of the CO spectral line, which has a typical full-width at half-maximum (FWHM) of ~0.7 MHz, and so are uniquely distinguishable from it."

Page 5, line 2. Change 'estimated uncertainties of 1 and 0.5 K respectively' to 'estimated uncertainties of 1 K and 0.5 K respectively'.
This has been changed.

Page 5, line 5. 'as a fraction of the a priori'. Which a priori?
This has been edited to clarify that the CO VMR is retrieved as a fraction of the CO a priori.

"CO VMRs are retrieved as a fraction of their a priori for numerical stability due the strong vertical gradients in atmospheric CO."

Page 5, line 5. Change 'due the strong gradients in atmospheric CO' to 'due to the strong gradients in atmospheric CO'. Are the CO gradients in the horizontal or vertical direction, or both?
Vertical. This is now clarified in the line.

"*CO VMRs are retrieved as a fraction of their a priori for numerical stability due to the strong vertical gradients in atmospheric CO.*"

2.3 CO profile characteristics

Page 5, line 8. 'The instrument required maintenance after this date…' After which date?
The sentence now indicates that it is the latter date in January.

Page 5, line 9. The unsmiley symbol on this line should probably be removed.
The emoji adds a culturally independent levity to the writing, without detracting from the scientific detail.

2.4 CO profile error estimates

Page 6, lines 5–6. 'An uncertainty of 1° is chosen for the pointing of the instrument to the sky, an overestimate of the motor uncertainty…' Could the actual pointing of the instrument be measured rather than relying on an output of the motor positioning mechanism? What is the motor referred to here?
The elevation angle of the instrument is measured at 21 degrees. This is indicated in Section 2.1. The sentence has been edited to clarify that the overestimation is to account for changes that might occur in the orientation of instrument table. The model of the motor is now included in the edited manuscript.
"An uncertainty of 1° is chosen for the pointing of the instrument to the sky, an overestimate of the motor (Faulhaber 3564K024B CS) uncertainty by an order of magnitude, to account for changes that may occur the orientation of the instrument table."

Section 2.1 now includes information on the measurement of the elevation angle.
"The alignment of the quasioptical components was checked using a laser positioned at the entrance to the cryocooler. The elevation angle of the instrument was measured using a self-levelling laser (Bosch GLL 3-80), which provides a horizontal line with an accuracy of 0.2 mm/m (0.2 mrad). Two horizontal lines, one directly from the laser and one passing through the quasioptical setup, were aligned on a screen approximately 5 m from the instrument. A sun scanning method has been used with other ground-based instruments to identify a pointing offset, e.g., for MIAWARA-C (Straub et al. 2010) and GROMOS-C (Fernandez et al., 2015), for which the offsets in the elevation angle were found to be 0.01° and 0.07°, respectively."

Page 6, line 11. 'uncertainty in the line position is ignored because the frequency grid used in the inversion can be shifted …' Presumably adjusting the frequency grid deals with Doppler line-shifts as well as uncertainty in the line position? Perhaps the wording should be 'is shifted' rather than 'can be shifted'?
Adjusting the frequency grid does not deal with doppler line shifts that are caused by winds at different altitudes, as they differ in direction and magnitude. CORAM does not have the spectral resolution to observe these changes. "can be shifted" has been changed to "is shifted".

3. Comparison with Aura MLS
Page 6, line 24. 'the upper limit of the MLS CO retrieval altitude …' At what altitude is the upper limit?
The preceding sentence states the pressure range of the data:

"The atmospheric pressure range of the data is 215 - 0.0046 hPa."

Page 6, line 25. 'The data has a positive bias in the middle atmosphere, compared to the ACE-FTS satellite instrument, of 20% …' Define 'ACE-FTS'. Change 'The data has …' to 'The data have …' Do you mean that the MLS CO VMR data are 20% higher than the corresponding ACE-FTS data?
The sentence has been edited to clarify these points:

"The data have a positive bias of 20% in the middle atmosphere (larger VMRs), compared to the Atmospheric Chemistry Experiment – Fourier Transform Spectrometer (ACE-FTS) satellite instrument (Livesey et al., 2015)."

Page 6, line 26. 'Pumphrey et al., 2007'. The reference is missing.
The reference has been added.

Page 6, line 26. 'subsequent versions showing a slight decrease in the CO VMR.' State what are the subsequent MLS CO data versions. Do you mean a slight decrease in CO VMR values or a decrease in the CO VMR bias compared to ACE-FTS? Or perhaps both?
The sentence mentions MLS data version 2.2, so subsequent data versions means ones that are after version 2.2. Listing versions of MLS data is superfluous information for the

manuscript. An interested reader may find information on the MLS website for datasets that are not used in this work. The MLS data quality document also refers to "later versions". Extra information has been included in the edited manuscript here to clarify that the MLS CO data since v2.2 has decreased in magnitude in the middle atmosphere, bringing the values closer to ACE-FTS.

"The data have a positive bias of 20% in the middle atmosphere (larger VMRs), compared to the Atmospheric Chemistry Experiment – Fourier Transform Spectrometer (ACE-FTS) satellite instrument (Livesey et al., 2015). This bias is estimated from a study of Version 2.2 of MLS CO data (Pumphrey et al., 2007), which showed a positive bias of 30 %. Subsequent versions of MLS CO, including the version used here, show a slight decrease in the CO VMR, bringing the values closer to those of ACE-FTS."

3.1 Colocated measurement comparison

Page 6, line 28. 'MLS measurements are subset to within ±2° latitude and ±10° longitude of CORAM'. Does this latitude/longitude range cover the location of the instrument on the ground and/or the CORAM observations in the middle atmosphere some distance away?
The sentence has been edited to read:

"MLS measurements are subset to within $\pm 2^\circ$ latitude and $\pm 10^\circ$ longitude of CORAM, calculated at 60 km altitude along the line of sight of CORAM (~ 156 km horizontally from the lab)."

Page 6, lines 28–29. 'The CO VMRs are expected to vary more in latitude than in longitude.' Why is this expected?
The atmospheric composition generally varies more in the meriodional direction compared to the zonal direction. This information is added to the line.

"The CO VMRs are expected to vary more in latitude than in longitude because the atmospheric composition generally varies more in the meridional direction compared to the zonal."

Page 6, line 29. 'A longitude space of ±5° was also tested …' should probably be 'A longitude space of ±5° was tested …'
This has been changed.

Page 6, line 30 – Page 7, line 1. 'Above 0.001 hPa, MLS CO profiles use a constant VMR value' should be 'Above 0.001 hPa, MLS CO profiles are constant in VMR value' or similar wording.
This has been changed,

Page 7, line 10. 'mid-November to mid-January'. Please give the specific dates.
This has been changed to *"November 19th to January 18th."*

Page 7, line 18. 'The correlation between KIMRA and MLS was slightly higher, …' Slightly higher than the correlation between which other instruments?
It is now clarified:

"The correlation between KIMRA and MLS was slightly higher than that for CORAM and MLS, remaining greater than 0.90 up to 82 km altitude."

Page 7, lines 21–22. 'after which the values become closer in VMR.' Please clarify - do you mean the MLS and CORAM profiles are in better agreement?
This has been clarified:

"The largest differences in CO are found at higher altitudes (≥68 km) in November and the first days of December, after which the values become closer in VMR, indicating better agreement between the instruments."

Page 7, lines 29 and 31. 'around December 22nd, leading to a local minimum in the first week of January' and 'for about the first 25 hours'. I wonder if the authors could be more exact in the timings?
This sentence has been removed and more detail is put into the description of the plot in Figure 8 that is a subset of the data. Descriptions for this plot are clearer for the reader.

4. CORAM data and usage
Page 7, line 29. 'decrease in middle-atmospheric CO' should be 'decrease in middle-atmospheric CO VMR'.
This sentence has been removed (see response to previous comment) and more detail is put into the description of the plot in Figure 8 that is a subset of the data. Descriptions for this plot are clearer for the reader.

Page 8, lines 2–3. 'Over this same time, between 60 and 70 km, there is an oscillation in the 4.1 and 6 ppmv contour lines, with peaks occurring every 1-2 hours.' Please could the authors provide some discussion of possible causes of the observed oscillation.
The beginning of the next paragraph in same section includes possible causes of the observed oscillations and provides citations to works that have analyzed similar features:

"These are broad descriptions of the data because one cannot fully characterise the variations in CO without the use of other data sources and model output. Variations on the timescales of an hour to weeks are visible in the data and require detailed study to elucidate the underlying dynamical processes, such as polar vortex shift, Rossby wave activity, SSW events, gravity wave perturbations (time scales of minutes to hours). Peridocities in trace gas data have previously been analysed using spectral decomposition techniques on ground-based measurements of water vapour and ozone (e.g., Struder et al., 2012, Hocke et al., 2013, Schranz et al., 2019) to identify waves with periods of days to weeks."

Page 8, lines 23–24. 'providing the averaging kernels do not significantly change over this time, which would change the measurement response.' Are the averaging kernels likely to change with time, and what might cause such changes?
The next sentence has been expanded to clarify.

"The measurement response for CORAM should not show significantly variation inside the retrievable altitude range but care should be taken at altitudes near the edges of the retrieval range of the profiles, where the measurement response has a strong gradient and can change quickly when there are rapid changes in CO concentrations at those altitudes."

Conclusion
Page 9, line 1. Suggest change 'CO profiles were retrieved …' to ''CO profiles were retrieved from observations …'
This has been edited to say "…retrieved from measurements…"

Page 9, lines 1–3. Suggest splitting this rather long sentence into two, e.g. with a full stop after '2017/2018' and starting the next sentence 'Error estimates…' It should be made clear that 'winter' refers to the northern hemisphere / Arctic. It would be worth restating in the conclusion the exact range of measurements dates.
The sentence has been broken into two and the dates added.

"CO profiles were retrieved from measurements in the Arctic winter of 2017/2018 (November 18th to January 19th). Error estimates show that the uncertainty in the temperature input for the inversions and the statistical noise on the spectrum are the largest contributions to the error budget, giving a maximum in the error profile of ~ 12 % of the a priori profile."

Page 9, lines 6–7. 'abnormally high CO measured by CORAM above ~ 68 km in November' should be rewritten as 'abnormally high CO VMR measured by CORAM above ~ 68 km in November 2017'.
This has been added.

Page 9, lines 9–10. 'November 2017 to January 2018 are currently available.' As suggested above, please give the exact dates for the dataset. How can the available data be accessed?
The dates have been added.
There is now a section on data availability.

References
The list of references appears to be sufficiently comprehensive and complete apart from the missing references for Pumphrey et al. (2007) and Kindlmann et al. (2002). However, the list should be carefully checked and correctly formatted by the authors.

Figures and Captions
Figure 2. Are the grid lines needed on the figures? Figure 2(a) should be replotted with a minimum of ~300 K on the receiver noise temperature axis.
The grid lines are thinner than the plotted data values and are a different colour so as not to be confused with the data.
This plot was provided by engineers during the testing phase and we do not have the original data to replot.

Figure 4. 'The measurement response (sum of the rows of the averaging kernels) divided by 4 is shown in solid blue.' There are a number of lines in the plot coloured blue. The colour scheme should be changed or the authors should make it clear whether the measurement response is shown by the thicker blue line.
It is now clarified that the measurement response is the thick solid blue line.

Figure 5. The axis label 'VMR [ppmv]' should be 'CO VMR [ppmv]'.
This has been changed.

Figure 6. The axis labels 'VMR' and 'Δ VMR' should be 'CO VMR [ppmv]' and 'Δ CO VMR [ppmv]' respectively. For Figure 6(d) the correlation scale needs to be changed to make better use of the plot, e.g. the range from 0.7 to 1.0.
These changes have been made.

Figure 7. Why were the selected altitudes chosen for plotting the time series? The axis labels 'VMR [ppmv]' should be 'CO VMR [ppmv]'. For Figure 7(a) the CO VMR scale should be adjusted to make better use of the plot, e.g. from 12 ppmv to 40 ppmv.
The altitudes span the retrieval altitude range in equal spacing. The changes have been made.

Figure 8. Perhaps the main plot might be clearer with the data gaps shown in white rather than black? Otherwise as presented the narrow black lines due to small data gaps look rather similar to the contour lines. The colourbar labels 'VMR [ppmv]' should be 'CO VMR [ppmv]'. Why were the particular CO VMR values chosen for the contours? The reference to Kindlmann et al. (2002) is missing. What is causing the gaps in the data record?
These changes have been implemented. The reference for Kindlmann et al. (2002) has been added.

Response to comments from Referee #2

This manuscript discusses middle atmospheric CO measurements carried out by a novel ground-based microwave spectrometer, CORAM, installed at the Arctic station of Ny-Ålesund (78.9◦N, 11.9◦E). The development of this instrument and its dataset are of interest to the scientific community, as CO is a useful tool for studying mesospheric dynamics in Polar regions and the satellite coverage of CO will become scarce in the near future. In fact, the creation of a network of ground-based instruments observing middle atmospheric constituents is desirable. The paper is well written and well organized and I recommend this work be published. In my opionion, however, since this is the presentation paper for CORAM, there are few aspects of the instrumentation and the data presented that should be better discussed in the manuscript. General comments The paper lacks information on the receiver itself, possibly a photo, a sketch of the quasi-optical front end, and on the observing equations of this (total power?) instrument. As a validation paper presenting a new receiver to the scientific community, I would expect there would be more data to show and that the validation would cover a longer time period. Especially since Polar mesospheric CO changes substantially from winter to summer, as do the observing capabilities of a 230 GHz ground-based instrument installed at sea level, so the data and their analysis results and uncertainties may change significantly from winter to summer. I understand that a technical failure occurred in January 2018 but now more than 14 months have passed. Are there new data to add to the analysis?

The local oscillator broke down in January. The Element became unstable and changed its frequency randomly and with a low frequency. At the measurement site we lack equipment to diagnose such a failure and asked the manufacturer to help in the diagnosis.
The production of a new element took another 12 months, hence we will be able to start measurements again in September 2019.

Specific comments

Page: 1
Sequence number: 1
Author:
Date: 12/04/2019 11:37:32
It's not clear what is intended with "precision" here. Would it be better to indicate the estimated total uncertainty instead?

The wording has been changed to uncertainty because the value from the estimated uncertainty in the profile is used here.

Page: 2
Sequence number: 1
Author:
Date: 12/04/2019 11:47:08
have been
This has been fixed.

Sequence number: 2
Author:
Date: 12/04/2019 11:51:35
The poor vertical resolution of the datasets could be a problem for studying gravity wave-induced fluctuations. Maybe a comment
on this aspect is needed.
The introduction now refers to the limited spatial resolution of the cited ground-based and satellite-borne instruments that have been used to study periodic fluctuations in trace gas profiles.

"The positive gradient of polar CO VMRs with altitude throughout the middle atmosphere, coupled with the time resolution of the presented measurement system at Ny-Ålesund ($\leq$ 1 hr), means that the dataset discussed here is well-suited to observing these periodic fluctuations, which are likely to be caused by vertical advection of air parcels by gravity waves (Zhu and Holton, 1997; Ekermann et al., 1998; Hocke et al., 2006). As with the ground-based and satellite-borne instruments in the works cited above, the analyses must be performed within the context of the limited spatial resolution of the measurements."

Page: 3
Sequence number: 1
Author:
Date: 12/04/2019 12:55:04
I would provide a photo of the instrument to have an idea of its front-end and how it is installed.
The photographs of the instrument do not offer clarity on the 3-dimensional optical bench. It is more likely to confuse the reader. A schematic of the front end in Figure 1 now includes

the main quasioptical components and beam paths for the signal, hot target, and cold target.

Sequence number: 2
Author:
Date: 19/04/2019 16:28:28
What materials were used for the window of the lab and the window of the cryocooler? Is it a total power instrument?
This information is now included in Section 2.1.

"CORAM is total-power radiometer housed at Ny-Ålesund, Svalbard (78.9°N, 11.9°E), and is part of the joint French-German Arctic Research Base, AWIPEV."

"The atmospheric signal enters the lab through a foam window that is transparent to millimetre-wave frequencies, and meets the pointing mirror of CORAM, …"

"After the pointing mirror, the atmospheric signal is directed by a series of quasioptical components through a mylar window in a cryocooler and fed into a corrugated horn antenna."

Sequence number: 3
Author:
Date: 19/04/2019 16:27:50
Authors should draw a sketch of this serie of mirrors, show how the signal is directed to the horn, and how they account for these
multiple reflections in their estimate of the elevation angle of their signal beam.
Figure 1 has been edited and now contains a simplified version of the quasioptics that demonstrates how the signal enters the horn from the pointing mirror.

The alignment is checked using a laser positioned at the entrance to the cryocooler. Section 2.1 now contains this information.

"Figure 1 shows a schematic drawing of the receiver including the components in the cryocooler, as well as a simplified version of the quasioptical layout The alignment of the quasioptical components was checked using a laser positioned at the entrance to the

cryocooler. The elevation angle of the instrument was measured using a self-levelling laser (Bosch GLL 3-80), which provides a horizontal line with an accuracy of 0.2 mm/m (0.2 mrad). Two horizontal lines, one directly from the laser and one passing through the quasioptical setup, were aligned on a screen approximately 5 m from the instrument. A sun scanning method has been used with other ground-based instruments to identify a pointing offset, e.g., for MIAWARA-C (Straub et al. 2010) and GROMOS-C (Fernandez et al., 2015), for which the offsets in the elevation angle were found to be 0.01° and 0.07°, respectively."

Sequence number: 4
Author:
Date: 12/04/2019 14:38:32
Does it enter the FFTS at 1.5 GHz?
Later on you write that the FFTS is the AC240 with a 1 GHz bandwidth, therefore the signal enters the FFTS at 500 MHz I guess. Is
this correct?
Yes, thank you. This has been fixed.

Sequence number: 5
Author:
Date: 12/04/2019 14:19:59
Why not writing the equation Tnoise = T1+T2/G1+T3/G4+...
This equation is now included in Section 2.1 to provide an estimate of the difference in noise temperature that comes with having an amplifier before the mixer.

"An estimate of the improvement in the receiver temperature (Janssen, 1993) can be made using a noise temperature cascade analysis. A variation of Friis' equation (Vowinkel, 1988) for two components in succession is $T = T_1 + T_2/G_1$, where T_1, and T_2 are the respective noise temperatures of the first and second components, G_1 is the linear gain of the first component, and T is the total noise temperature. The noise temperature of the LNA plus waveguide filter was measured to be 1350 K at room temperature, and the linear gain was measured at 158 (corresponding to 22 dB) (Fig. 2b). The noise temperature of the sub-harmonic mixer is ~ 1500 K at room temperature and has a linear gain of ~ 0.16 (corresponding to -8 dB). Applying Friis' equation with the LNA preceding the mixer gives a noise temperature of ~ 1360 K. The same calculation with the mixer as the first component gives a noise temperature of ~ 9800 K. The dominant contribution to the noise temperature of CORAM is from the LNA/filter/mixer. Cooling the components can considerably reduce

their noise temperature. Figure 2b shows the noise temperature and gain of the LNA + filter, measured at room temperature. Figure 2c shows the receiver temperature for CORAM measured at the exit of the cryocooler, with the cryocooler components at a typical temperature of 39 K. At 8.5 GHz, the receiver temperature is below 350 K. Figure 2a shows the frequency response of the waveguide filter with a suppression of ~ -45 dB at 213.5 GHz."

Sequence number: 6
Author:
Date: 12/04/2019 14:15:57
do you mean "lower cost"?
"cost" has been changed to "price" here.

Sequence number: 7
Author:
Date: 12/04/2019 14:23:19
I would write the equation that relates the receiver noise to the system noise, to make clear the difference between the two parameters.
Equations have been added to this section to clarify the difference between the receiver temperature and the system temperature. The radiometer equation is also included to relate the system temperature to the integration time.

"The system temperature can be described as $T_{sys} = T_{rec} + T_a$ (Parrish et al., 1988, Janssen, 1993, Stanimirović et al., 2002). The receiver temperature, T_{rec}, considers the contributions from CORAM, and the antenna temperature, T_a, considers the contributions from the atmospheric background and signal being measured. The system temperature is related to the measurement time through the so-called radiometer equation: $\sigma_T = T_{sys} / (Bt)^{1/2}$, where σ_T is the statistical noise on a measured spectrum, B is the frequency bandwidth of the measurement, and t is the integration time for the measurement."

Page: 4
Sequence number: 1
Author:
Date: 12/04/2019 14:40:49
I would add a short description of the observing equations (total power, correct?) and how the main unknowns in the equation are

estimated/measured.
Section 2 has been edited to include a description of the inversion problem and how it relates to the measurements made with CORAM:

"2.2.1 Defining the inversion problem

Schwarzchild's equation describes radiative transfer through a medium in local thermodynamic equilibrium. In the millimetre-wave region, at a given frequency, the measured intensity can be expressed in terms of brightness temperature, T_b, where

$$T_b = T_{b_0} e^{-\tau(l_0)} + \int_0^{l_0} T(l)\alpha(l) e^{-\tau(l)} dl, \quad (1)$$

with l denoting the path through the atmosphere from a point l_0 to the measurement point at l = 0. The initial intensity is T_{b_0}, the optical depth of the atmosphere is described by τ, and the absorption coefficient is defined as α. More details can be found in Janssen (1993) and references therein. T_b in equation (1), as a function of frequency, is generally the mathematical description of the calibrated atmospheric spectrum, the antenna temperature (T_a) from Sect. 2.1. For a total power radiometer such as CORAM, the calibrated antenna temperature is found using:

$$T_a = \left(\frac{V_{atm} - V_c}{V_h - V_c}\right)(T_h - T_c) + T_c, \quad (2)$$

where T_h and T_c are the temperatures of the hot and cold calibration targets (Sect. 2.1), V_h and V_c are the measured voltages when observing the hot and cold targets, respectively. V_{atm} is the measured voltage when observing the atmosphere.
The desired quantity, the VMR of a trace gas, is contained within the description of the absorption coefficient, α. Equation (1) must be inverted to retrieve this information. The form of Equation (1) is that of a Fredholm integral of the second kind and is inherently sensitive to small perturbations (like noise on a spectrum). To overcome this, the numerical inversion here is performed iteratively using a maximum a posterieri probability estimation.

2.2.2 Inversion method

Altitude profiles of CO VMR are retrieved from the measured spectra using an optimal estimation inversion technique (Rodgers, 2000). The method uses some a priori information of the state of the atmosphere to constrain the profile that is retrieved from the measured spectrum. The linear solution to the inversion problem can be expressed as $\hat{\boldsymbol{x}} = \boldsymbol{A}\boldsymbol{x} + (\boldsymbol{I} - \boldsymbol{A})\boldsymbol{x_a}$, *where* $\hat{\boldsymbol{x}}$ *is the retrieved state vector (VMR profile),* $\boldsymbol{x}$ *is the true atmospheric state vector,* $\boldsymbol{x_a}$ *is the a priori state vector, and* $\boldsymbol{I}$ *is the identity matrix.* $\boldsymbol{A}$ *is the averaging kernel matrix, which describes the sensitivity of a retrieved state to the true state*

(Rodgers, 2000). The sensitivity of the retrieved state at altitude i, to the true state at altitude j, is given by $\boldsymbol{A_{ij}} = \partial \hat{\boldsymbol{x}}_i / \partial \boldsymbol{x}_j$*."*

Sequence number: 2
Author:
Date: 12/04/2019 15:38:21
Given the large seasonal variability of mesospheric CO over polar regions, what will you do with summer data? Since you're
describing an instrument that is designed for long-term measurements you should plan for an entire year of data analysis.
The CO concentrations during the summer are very low and are not detectable by CORAM. Clarification on this is now included in the abstract and in Section 2.1.

Sequence number: 3
Author:
Date: 03/04/2019 13:02:25
This is true only if you consider the central part of the spectral line and not its broad wings which are produced from the emission of
stratospheric CO.
A new line has been added directly after this to clarify that the broad wings of the spectral line are produced at altitudes lower than the retrievable altitude limit of CORAM.

"The broad wings of a CO spectral line are produced by CO molecules at altitudes below the retrievable altitude limit of CORAM (approximately 47 km, see Sect. 2.3)."

Sequence number: 4
Author:
Date: 15/04/2019 16:14:11
it would be useful to see an example of the sinewaves that are being removed
An example of the fit to the baseline is included in Figure 3.

Page: 5
Sequence number: 1
Author:
Date: 03/04/2019 15:06:58
It's not clear whether the spectrum showed had already the sinewaves subtracted or not

The spectrum shown is the original measurement. The fit to the baseline (baseline fit), which includes the sinewaves, forms part of the inversion fit. The baseline fit is not separately subtracted from the measurement.
The caption to Figure 3 has been edited to emphasise that the baseline fit in the lower panel is a part of the overall fit shown in the upper panel.

From Section 2.2
"Qpack2 provides the capability to fit a series of functions to the baseline of the measured spectra (a baseline fit) to account for errors in the baseline which are likely caused by standing waves in the instrument. The baseline fit is included in the optimal estimation and forms part of the overall fit to the measurement (inversion fit)."

"Figure 3: (a) Upper: an example spectrum measured by CORAM on Dec 24th 2017 between 20:04 and 21:03 UTC. The inversion fit to the measurement is shown (smoother red line). Lower: the residual of the measurement and the inversion fit (solid black line). The dashed red line shows the baseline fit for the inversion, which is part of the inversion fit shown in the upper panel (Sect. 2.2). (b) The CO profile retrieved from the measurement (solid blue) and the a priori profile that is used as input to the inversion (dashed black)."

Sequence number: 2
Author:
Date: 15/04/2019 17:38:50
I think authors should be a little more precise here
Section 2.2 has been edited to contain a more detailed description of the averaging kernels.

"Altitude profiles of CO VMR are retrieved from the measured spectra using an optimal estimation inversion technique (Rodgers, 2000). The method uses some a priori information of the state of the atmosphere to constrain the profile that is retrieved from the measured spectrum. The linear solution to the inversion problem can be expressed as $\hat{\boldsymbol{x}} = \boldsymbol{A}\boldsymbol{x} + (\boldsymbol{I} - \boldsymbol{A})\boldsymbol{x}_a$, *where* $\hat{\boldsymbol{x}}$ *is the retrieved state vector,* $\boldsymbol{x}$ *is the true atmospheric state vector,* $\boldsymbol{x}_a$ *is the a priori state vector, and* $\boldsymbol{I}$ *is the identity matrix.* $\boldsymbol{A}$ *is the averaging kernel matrix, which describes the sensitivity of a retrieved state to the true state (Rodgers, 2000). The sensitivity of the retrieved state at altitude i, to the true state at altitude j, is given by* $\boldsymbol{A}_{ij} = \partial \hat{\boldsymbol{x}}_i / \partial \boldsymbol{x}_j$."

Sequence number: 3
Author:
Date: 15/04/2019 17:40:41
It's unclear to me how you can reach a 87 km altitude limit considering the Doppler broadening and with a 61 kHz channel resolution.
The averaging kernels, which describe the distribution of sensitivity of the instrument are used. Section 2.3 outlines that a measurement response of 0.8 is often used to determine the altitude range of an instrument, as is done here. Later in Section 2.3, the peaks of the averaging kernels are discussed, and how this affects the interpretation of the CO profiles above ~70 km. This topic is discussed in more detail in Hoffmann et al. (2011) for ground-based CO measurements and this is also cited in Section 2.3.

"A common way to estimate the altitude limits of a retrieved profile is to define the sum of the rows of the averaging kernels as the measurement response and assign a cut-off value. The choice of the cut-off value is rather arbitrary but 0.8 is regularly used (e.g., Forkmann et al., 2012; Straub et al., 2013, Schranz et al., 2018), and is also used here. With the above definitions, the CO profiles from CORAM during winter 2017/2018 have an average altitude range of approximately 47 – 87 km, with an average altitude resolution varying between approximately 12.5 and 28 km over that range. The retrieval range can change depending on the distribution of CO in the atmosphere (the lower limit can decrease in altitude when there are higher CO values at lower altitudes) and the value provided here is the mean range over the time span of the data.
The retrieval limits will vary from measurement to measurement and individual profiles should be considered in combination with the accompanying averaging kernels. The centres of the averaging kernels, when represented in VMR, are shifted down in altitude compared to a representation in relative units (Hoffmann et al., 2011). The lower limit of the retrieval here is defined by the SNR in the measurement and the upper limit is set by a transition from a pressure broadening regime to a doppler broadening one. The result of this change is that, above approximately 70 km in the VMR representation, the centres of the averaging kernels do not increase in altitude with their corresponding retrieval altitudes. The retrieved CO values above ~ 70 km altitude do contain information from the atmosphere that corresponds with the retrieval altitude, but the VMR representation of the profile should be considered with care. Hoffmann et al. (2011) provides a detailed discussion on the representation of data for ground-based CO measurements. Hoffmann emphasises that the limited vertical resolution of the data must be taken into account for the use and interpretation of the data

by considering each realisation of the averaging kernels, and so the a priori and averaging kernels form an essential part of the dataset."

Sequence number: 4
Author:
Date: 03/04/2019 15:26:27
Call figure 4
This has been added.

Sequence number: 5
Author:
Date: 15/04/2019 17:56:15
This sentence is unclear to me. As I see it, upwards of 70 km altitude you can't retrieve a profile anymore but have basically a
partial column content. This suggests that on top of using the measurement response between 0.8 and 1.2 in order to identify the
altitude range where the data sets is reliable, you should possibly use also the close correspondence between nominal and retrieval altitudes.
The area under the averaging kernels (the sum of the rows) is used to define a limit. Then, later in Section 2.3, the correspondence between 'nominal and retrieval altitudes' is discussed. The location of peaks of the averaging kernels are discussed, and how this affects the interpretation of the CO profiles above ~70 km. This topic has been covered in more detail in Hoffmann et al. (2011) for ground-based CO measurements and this is also cited in Section 2.3.
"The retrieval limits will vary from measurement to measurement and individual profiles should be considered in combination with the accompanying averaging kernels. The centres of the averaging kernels, when represented in VMR, are shifted down in altitude compared to a representation in relative units (Hoffmann et al., 2011). The lower limit of the retrieval here is defined by the SNR in the measurement and the upper limit is set by a transition from a pressure broadening regime to a doppler broadening one. The result of this change is that, above approximately 70 km in the VMR representation, the centres of the averaging kernels do not increase in altitude with their corresponding retrieval altitudes. The retrieved CO values above ~ 70 km altitude do contain information from the atmosphere that corresponds with the retrieval altitude, but the VMR representation of the profile should be considered with care. Hoffmann et al. (2011) provides a detailed discussion on the representation of data for ground-based CO measurements. *Hoffmann emphasises that the*

limited vertical resolution of the data must be taken into account for the use and interpretation of the data by considering each realisation of the averaging kernels, and so the a priori and averaging kernels form an essential part of the dataset."

To make this clearer to the reader, the caveats on altitude range are now also included in both the abstract and the conclusion.

Abstract:
"The profiles in the current dataset have an average altitude range of 47-87 km, with special consideration to be given to data at > ~70 km altitude."

Conclusion:
"The mean of the averaging kernel matrix for the CORAM dataset gives an average retrieval altitude range of 47-87 km with an average altitude resolution of 12.5 to 28 km over this range. Data at higher altitudes should be treated with care as the VMR representation of the averaging kernels do not peak at the corresponding retrieval grid points above ~70 km altitude."

Page: 6
Sequence number: 1
Author:
Date: 19/04/2019 18:02:11
This sentence suggests that the pointing azimuth of the instrument is unknown. Could you please clarify? Please explain how you
measure the elevation angle of the signal beam, how you set the zero elevation. Do you perform a sun scan? Authors write "The
atmospheric signal enters the lab at 20° elevation
and is directed by a series of mirrors through a window in a cryocooler". How do you measure the elevation angle above the
horizon of your beam?
The sentence has been edited to clarify that the overestimate is used to account for changes that may occur in the orientation of the instrument table.
"An uncertainty of 1 ° is chosen for the pointing of the instrument to the sky, an overestimate of the motor (Faulhaber 3564K024B CS) uncertainty by an order of magnitude, to account for changes that may occur in the orientation of the instrument table."

Section 2.1 now includes information on the measurement of the elevation angle.
"The alignment of the quasioptical components was checked using a laser positioned at the entrance to the cryocooler. The elevation angle of the instrument was measured using a self-levelling laser (Bosch GLL 3-80), which provides a horizontal line with an accuracy of 0.2 mm/m (0.2 mrad). Two horizontal lines, one directly from the laser and one passing through the quasioptical setup, were aligned on a screen approximately 5 m from the instrument. A sun scanning method has been used with other ground-based instruments to identify a pointing offset, e.g., for MIAWARA-C (Straub et al. 2010) and GROMOS-C (Fernandez et al., 2015), for which the offsets in the elevation angle were found to be 0.01° and 0.07°, respectively."

Sequence number: 2
Author:
Date: 19/04/2019 11:17:37
Are there temperature sensors measuring the various temps?
This is now clarified in Section 2.1.

"The measured signal is calibrated using two blackbody targets at known temperatures (measured with mounted sensors): a cold target in the cryocooler at ~ 70 K and a warm target at ~ 293 K."

Sequence number: 3
Author:
Date: 03/04/2019 15:25:30
Somewhere here there should be a call to Figure 5
Figure 5 is called on line 13 of the original manuscript.
"The error estimates, including the average of the error arising from statistical noise on the spectrum, are plotted in Fig. 5."

Page: 7
Sequence number: 1
Author:
Date: 19/04/2019 18:03:04
This smoothing process involves the CORAM apriori profile as well. For this reason, you cannot really calculate a correlation

coefficient between the MLS smoothed profiles and CORAM profiles as if the two datasets were independent. If you wish to do so, you should use the MLS original profiles or perform a smoothing process of MLS profiles which does not involve CORAM AVK or apriori.
The correlation between the unsmoothed MLS data and CORAM data is now included in Figure 6. Section 3.1 has been edited to include the following.

"After smoothing, the MLS and CORAM data are not truly independent, so the correlation of CORAM with the unsmoothed MLS data is also calculated and shows more variation over the retrievable altitude range, with a minimum of 0.59 and a maximum of 0.81."

Page: 9
Sequence number: 1
Author:
Date: 19/04/2019 12:45:25
I am uncomfortable with the overall statement that the valid altitude range for the retrieval is up to 87 km when it is well known that
above about 70 km altitude the Doppler broadening takes over and you cannot obtain a vertical distribution of CO from its line
shape.
To clarify, the caveats on altitude range are now also included in both the abstract and the conclusion.

Abstract:
"The profiles in the current dataset have an average altitude range of 47-87 km, with special consideration to be given to data at > ~70 km altitude."

Conclusion:
"The mean of the averaging kernel matrix for the CORAM dataset gives an average retrieval altitude range of 47-87 km with an average altitude resolution of 12.5 to 28 km over this range. Data at higher altitudes should be treated with care as the VMR representation of the averaging kernels do not peak at the corresponding retrieval grid points above ~70 km altitude."

Sequence number: 2
Author:

Date: 19/04/2019 12:56:52
If you degrade MLS using CORAM averaging kernels and apriori the two datasets are then not independent and you can't really
talk about their "correlation". See earlier comment.
The statement has been edited to include information on the smoothed and unsmoothed data.

"Correlations between the instruments range from 0.80 to 0.92 over CORAMs retrievable altitude range for MLS data smoothed with the CORAM averaging kernels, and from 0.59 to 0.81 when using the unsmoothed MLS data."

Page: 15
Sequence number: 1
Author:
Date: 03/04/2019 12:23:03
Remove "in"
This has been fixed.

Sequence number: 2
Author:
Date: 12/04/2019 14:23:52
why was this measurement carried out at 8.5 GHz and not at the FFTS?
The measurement was made by RPG as part of the production process for the new components. The system temperature of CORAM of ~600 K is now also included in the caption.

Page: 16
Sequence number: 1
Author:
Date: 03/04/2019 13:07:32
I do not understand whether the dashed red line represents what was subtracted from the original spectrum. Authors should
explain/show this subtraction a little better as this is always a touchy topic.
The dashed red line is the fit to the baseline that is included in the inversion fit (the overall fit of the line). A separate subtraction is not made and is purposefully not mentioned in the

description in Section 2.2 nor in the caption to Figure 3. It is now emphasized in the caption that the baseline fit is a part of the inversion fit shown in the upper panel.

From Section 2.2
"Qpack2 provides the capability to fit a series of functions to the baseline of the measured spectra (a baseline fit) to account for errors in the baseline which are likely caused by standing waves in the instrument. The baseline fit is included in the optimal estimation and forms part of the overall fit to the measurement (inversion fit)."

"Figure 3: (a) Upper: an example spectrum measured by CORAM on Dec 24th 2017 between 20:04 and 21:03 UTC. The inversion fit to the measurement is shown (smoother red line). Lower: the residual of the measurement and the inversion fit (solid black line). The dashed red line shows the baseline fit for the inversion, which is part of the inversion fit shown in the upper panel (Sect. 2.2). (b) The CO profile retrieved from the measurement (solid blue) and the a priori profile that is used as input to the inversion (dashed black)."

Page: 17
Sequence number: 1
Author:
Date: 15/04/2019 16:45:24
In my understanding measurement response values larger than 1.2 are as critical as those below 0.8. Is this correct?
The measurement response can be thought of as a rough measure of the fraction of the retrieved state that comes from the data, instead of from the a priori. That is why it is often used to determine a cutoff where the data contribution is considered too little. It is only a rough measure though, as seen, and as you pointed out, by the measurement response often exceeding 1 at some altitudes.

More information has been added to Section 2.3 and reference to Rodgers (2000) and Payne et al. (2009).
"The measurement response can generally be thought of as a rough measure of the fraction of the retrieved state that comes from the data, rather than the a priori (Rodgers., 2000). As noted by Payne et al. (2009), this is only a rough measure, and the measurement response often exceeds 1 at some altitudes."

Page: 18

Sequence number: 1
Author:
Date: 19/04/2019 18:04:53
I am very surprised that a pointing uncertainty of 1° leads to such a small uncertainty in the retrieved profile.
The calculations were checked and the same result was found. It is likely that the pointing is more critical for systems that use a tipping curve method to calculate the atmospheric opacity for use in correcting the measured spectrum. And also for systems that use atmospheric measurements at one or more specific angles as the hot/cold targets to calibrate the signal data.

Page: 20
Sequence number: 1
Author:
Date: 19/04/2019 18:19:27
I think authors should show these time series at various altitudes so that the reader can better evaluate the difference between
CORAM and MLS datapoints. The vertical scales here are so different from altitude to altitude that it is really difficult to grasp useful
info.
It is unclear what is meant here. The time series is shown at 5 altitudes between 48 and 88 km. To clarify, the figure caption has been expanded to include the specific altitudes.

"Figure 7: Time series of the daily CORAM and MLS CO VMR values at altitudes of 48, 58, 68, 78, and 88 km."

Ground-based millimetre-wave measurements of middle-atmospheric carbon monoxide above Ny-Ålesund (78.9° N, 11.9° E)

Niall J. Ryan[1], Mathias Palm[1], Christoph G. Hoffmann[2], Jens Goliasch[3], Justus Notholt[1]

[1]Institute of Environmental Physics, University of Bremen, Bremen, 28359, Germany
[2]Institute of Physics, University of Greifswald, Felix-Hausdorff-Str. 6, 17489, Greifswald, Germany
[3]RPG-Radiometer Physics GmbH, Werner-von-Siemens-Str. 4, 53340 Meckenheim, Germany

Correspondence to: Niall J. Ryan (n_ryan@iup.physik.uni-bremen.de)

Abstract. We present a new ground-based system for measurements of middle-atmospheric carbon monoxide (CO) at Ny-Ålesund, Svalbard, and the altitude profiles of CO volume mixing ratios (VMR) measured during the 2017/2018 winter. The Carbon Monoxide Radiometer for Atmospheric Measurements (CORAM) records spectra from CO spectral emissions in the middle-atmosphere with the aid of a low-noise amplifier designed for the 230 GHz spectral region. Altitude profiles of CO VMRs are retrieved from the measured spectra using an optimal estimation inversion technique. The profiles in the current dataset have an average altitude range of 47-87 km, with special consideration to be given to data at > ~70 km altitude. Theand an estimated precision uncertainty in the CO profile peaksking at ~ 12 % of the a priori used in the inversion. The CORAM profiles are compared to collocated CO measurements from the Microwave Limb Sounder (MLS) aboard the Aura satellite and show a difference of 7.4 – 16.1 %, with a maximum absolute difference of 2.5 ppmv at 86 km altitude. CO profiles are currently available at 1 hr resolution between November 2017 and January 2018. The instrument measures during Arctic winter because summer-time CO concentrations are so low as to be undetectable by CORAM.

1 Introduction

Millimetre-wave (also referred to as microwave) rRadiometers are powerful tools for measuring the composition of the atmosphere. This is particularly true for areas where there are prolonged night-time periods, such as the poles. Radiometers The instruments can measure emissions from molecules in the atmosphere, thus in contrast to solar absorption measurements that relyremoving any reliance on the sun. Coherent detection of the atmospheric signal, achieved through heterodyne receivers, and eElectronic manipulation of that signal,of the measured atmospheric signal makes it possible to detect and resolve signals spectral lines with very low intensities, especially when the electronics are cooled to low temperatures, thus producing lower thermal noise (Janssen, 1993). Ground-based measurements in the thermal IR band generally do not have the capability to distinguish the mesospheric and stratospheric parts of the carbon monoxide (CO) profile (Kasai et al., 2005; Velazco et al., 2007).

Altitude profiles of carbon monoxide (CO) concentrations in the middle atmosphere are useful in quantifying dynamical processes. Because the lifetime of CO during polar night is on the order of months (Solomon et al., 1985; Allen et al., 1999),

it is a good tracer for atmospheric dynamics. The generally increasing volume mixing ratio (VMR) of CO with altitude has a strong gradient, which helps to identify the origin of increases or decreases in concentration. DAn example of this is during polar night, when CO concentrations increase in the middle atmosphere due to the vertical branch of the residual mean circulation bringing CO-rich air from higher altitudes (Smith et al., 2011; Garcia et al., 2014). Similarly, a decrease in middle-atmospheric CO in polar spring is linked to a change in direction of the residual mean circulation at this time. The breakup of the polar vortex in spring also allows for more CO-poor air to be transported poleward from lower latitudes (Manney et al., 2009; 2015), adding complexity to the quantitative link between dynamical processes and variations in CO. Changes in CO (and other tracers) VMRs can be caused by chemical production/loss (night-time CO is lost through reaction with a layer of hydroxyl at ~ 82 km (Solomon et al., 1985; Brinksma et al., 1998; Damiani et al., 2010; Ryan et al., 2018)), and by dynamical processes: vertical/horizontal advection, eddy transport, and to a lesser extent, molecular diffusion (Garcia and Solomon, 1983; Andrews et al., 1987, Brasseur and Solomon, 2005; Smith et al., 2011). While vertical advection is, in general, the dominating process, modelling studies of middle-atmospheric CO indicate that the vertical transport rates calculated from trace gas measurements do not accurately represent the mean descent/ascent of the atmosphere because the 'true' effect of vertical advection is masked by other processes (Hoffmann, 2012; Ryan et al., 2018).

The general increase in middle-atmospheric CO VMR during polar night is seen in multiple datasets (e.g., Allen et al., 2000, Forkman et al., 2005, Funke et al., 2009, Hoffmann et al., 2011, Ryan et al 2017), and the phenomenon has been observed for other tracers, e.g., H_2O (Lee et al., 2011; Straub et al., 2012), N_2O, CH_4, and H_2O (Nassar et al., 2005), and NO, CH_4, and H_2O (Bailey et al., 2014). The calculated rates of vertical tracer transport in the above studies range from -1200 to +450 m/day (negative numbers indicate descent), with the values representing varying averages in space and/or time. Variations in tracer VMRs on smaller timescales (minutes to hours) can be caused by waves that displace air parcels from their equilibrium positions and perturb trace gas profiles (e.g. Zhu and Holton, 1997; Ekermann et al., 1998; Fritts and Alexander, 2003; Noguchi et al., 2006; Chane Ming et al., 2016). Data from ground-based radiometers with relatively high time resolution (order of an hour or less) have been used to investigate small periodic fluctuations in ozone (O_3) and water vapour (Hocke et al., 2006;; Moreira et al., 2018;; Schranz et al., 2018). The positive gradient of polar CO VMRs with altitude throughout the middle atmosphere, coupled with the time resolution of the presented measurement system at Ny-Ålesund (≤-1 hr), means that the dataset discussed here is well-suited to observing these periodic fluctuations, which are likely to be caused by vertical advection of air parcels by gravity waves (Zhu and Holton, 1997; Ekermann et al., 1998; Hocke et al., 2006). As with the ground-based and satellite-borne instruments in the works cited above, the analyses must be performed within the context of the limited spatial resolution of the measurements.

The Kiruna Microwave Radiometer, KIMRA, is also currently making measurements of middle-atmospheric CO at 67.8° N (Raffalski et al, 2005; Hoffmann et al., 2011; Ryan et al., 2017), and the addition of a new instrument at Ny-Ålesund provides a needed increase in Arctic coverage and an excellent opportunity for comparison of CO at locations near the polar vortex edge and inside the vortex, particularly during dynamic events such as sudden stratospheric warmings (SSWs). CO profiles from satellite measurements have been used regularly to study processes in the polar winter atmosphere (e.g.

Damiani et al., 2014; Lee et al., 2011; Manney et al., 2009; McLandress et al., 2013), but recent ground-based CO datasets in the polar (and nearby) regions have been sparse: The Onsala Space Observatory instrument (57° N, 12° E) (Forkman et al., 2012), which produced data for 2002 – 2008, and from 2014; The ground-based millimetre-wave spectrometer (GBMS) at Thule Air Base (76.5° N, 68.7° W), used to investigate the Arctic winter of 2001/2002 (Muscari et al., 2007) and the sudden stratospheric warming (SSW) in 2009 (Di Biagio et al., 2010); The British Antarctic Survey (BAS) radiometer data at Troll Station (72° S, 2.5° E) covers February 2008 to January 2010 (Straub et al., 2013). These instruments also measure the rotational transitions of CO and can operate during polar night.

The high time resolution of the CO Radiometer for Atmospheric Measurements (CORAM) is achieved primarily with a high-frequency low-noise amplifier (LNA), which operates on the atmospheric CO signal at 230.54 GHz before the signal is mixed with the radiometer's local oscillator. CORAM is discussed in Section 2, as well as the inversion method, CO profile characteristics, and error estimates. Section 3 shows the results of a comparison with collocated data from the Microwave Limb Sounder (MLS). Section 4 shows the CORAM profile timeseries and discusses the usage of the data, and Section 5 offers some concluding remarks.

2 Instrument and measured data

2.1 CORAM

CORAM is a total-power radiometer housed at Ny-Ålesund, Svalbard (78.9° N, 11.9° E), and is part of the joint French-German Arctic Research Base, AWIPEV. CORAM measures the J = 2 → 1 rotational transition of CO at 230.54 GHz. The instrument was installed in 2017 and made first measurements of CO in the winter of 2017/2018. During the summer period, middle-atmospheric concentrations of CO are so small that they are not detectable by CORAM. The atmospheric signal enters the lab through a foam window that is transparent to millimetre-wave frequencies, and meets the pointing mirror of CORAM, angled at 21~~0~~° elevation. This angle was chosen by performing a series of atmospheric radiative transfer simulations at different elevation angles, using a climatological polar winter atmosphere, and determining which angle provided the strongest CO spectral line. The choice of angle is a trade-off of maximum path length through the target gas in the atmosphere, and minimum attenuation of the target signal by atmospheric water vapour that is primarily in the troposphere. The azimuth angle of the atmospheric signal is 113°, defined by the laboratory in which CORAM is held. After the pointing mirror, the atmospheric signal ~~and~~ is directed by a series of quasioptical components~~mirrors~~ through a mylar window in a cryocooler and ~~,~~ fed into a corrugated horn antenna. The quasioptical setup has an antenna pattern with a half-power-beam-width of ~ 5°. After the horn, the signal is~~and~~ amplified by a 230 GHz LNA. The unwanted sideband at ~ 213.5 GHz is supressed with a waveguide filter before the ~~atmospheric~~ signal is mixed with the local oscillator (LO) signal (111 GHz) using a sub-harmonic mixer. Now at an intermediate frequency of 8.5 GHz, the signal exits the cooler and is

amplified with another LNA before being further downconverted to 0~~1~~.5 GHz and analysed by a Fast Fourier Transform Spectrometer (FFTS).

~~-~~Figure 1 shows a schematic drawing of the receiver including the components in the cryocooler, as well as a simplified version of the quasioptical layout. The alignment of the quasioptical components was checked using a laser positioned at the entrance to the cryocooler. The elevation angle of the instrument was measured using a self-levelling laser (Bosch GLL 3-80), which provides a horizontal line with an accuracy of 0.2 mm/m (0.2 mrad). Two horizontal lines, one directly from the laser and one passing through the quasioptical setup, were aligned on a screen approximately 5 m from the instrument. A sun scanning method has been used with other ground-based instruments to identify a pointing offset, e.g., for MIAWARA-C (Straub et al. 2010) and GROMOS-C (Fernandez et al., 2015), for which the offsets in the elevation angle were found to be 0.01° and 0.07°, respectively.

The measured atmospheric signal is calibrated using two blackbody targets at known temperatures (measured with mounted sensors): a cold target in the cryocooler at ~ 70 K and a warm target at ~ 293 K. The integration time for each blackbody is the same as that for the atmospheric signal. A path length modulator is part of the setup that directs the atmospheric signal to the feedhorn, in order to reduce the amplitude of any standing waves in the quasioptics. The FFTS is an Acqiris AC240 and has a bandwidth of 1 GHz with 16384 channels, providing ~61 kHz resolution. A high spectral resolution, depending on the Doppler width of a spectral line (~300 kHz in this case), is required for resolving the mesospheric contribution to the spectrum. CORAM performs the Fourier Transform in real time and the fully resolved spectrum is stored. The cryocooler makes use of a CTI Cryogenics 350 CP coldhead and a CTI Cryogenics 8200 compressor, as well as a helium cooling machine. ~~Figure 2a shows the frequency response of the waveguide filter with a suppression of > 45 dB at 213.5 GHz.~~

Each electronic component in a signal chain will add noise to the atmospheric signal of interest, which will also be amplified with any subsequent amplifiers. Because of the better~~greater~~ availability/price~~cost~~/quality of amplifiers that operated at several GHz, radiometers used for atmospheric measurements at frequencies > ~200 GHz have generally employed LNAs after the atmospheric signal has been mixed with the LO and has been downconverted to a lower frequency. The first LNA in CORAM, produced by Radiometer Physics GmbH (RPG), operates at a relatively high frequency of 230 GHz and allows for the atmospheric signal to be amplified before it encounters the mixer, ultimately providing an increased signal-to-noise ratio (SNR) for an atmospheric measurement. This configuration has been used before for similar instruments e.g., MIAWARA-C and GROMOS-C, which measure water vapour at 22 GHz, and ozone at 110 GHz, respectively.

An estimate of the improvement in the receiver temperature (Janssen, 1993) can be made using a noise temperature cascade analysis. A variation of Friis' equation (Vowinkel, 1988) for two components in succession is $T = T_1 + T_2/G_1$, where T_1, and T_2 are the respective noise temperatures of the first and second components, G_1 is the linear gain of the first component, and T is the total noise temperature. The noise temperature of the LNA plus waveguide filter was measured to be 1350 K at room temperature, and the linear gain was measured at 158 (corresponding to 22 dB) (Fig. 2b). The noise temperature of the sub-harmonic mixer is ~ 1500 K at room temperature and has a linear gain of ~ 0.16 (corresponding to -8 dB). Applying Friis' equation with the LNA preceding the mixer gives a noise temperature of ~ 1360 K. The same calculation with the mixer as

the first component gives a noise temperature of ~ 9800 K. The dominant contribution to the receiver temperature of CORAM is from the LNA/filter/mixer. Cooling the components can considerably reduce their noise temperature. Figure 2b shows the noise temperature and gain of the LNA + filter, measured at room temperature. Figure 2c shows the receiver temperature for CORAM measured at the exit of the cryocooler, with the cryocooler components at a typical temperature of 39 K. At 8.5 GHz, the receiver temperature is below 350 K. Figure 2a shows the frequency response of the waveguide filter with a suppression of ~ -45 dB at 213.5 GHz.

~~The measurement time needed to produce a spectrum with a desired SNR is proportional to the square of the system noise temperature, which also includes contributions from the second downconversion, the atmospheric background and signal, and quasioptical spillover (Parrish et al., 1988, Janssen, 1993, Stanimirović et al., 2002).~~The system temperature can be described as $T_{sys} = T_{rec} + T_a$ (Parrish et al., 1988; Janssen, 1993; Stanimirović et al., 2002). The receiver temperature, T_{rec}, considers the contributions from CORAM, and the antenna temperature, T_a, considers the contributions from the atmospheric background and signal being measured. The system temperature is related to the measurement time through the so-called ideal radiometer equation: $\sigma_T = T_{sys} / (Bt)^{1/2}$, where σ_T is the statistical noise on a measured spectrum, B is the frequency bandwidth of the measurement, and t is the integration time for the measurement. This relationship determines the measurement time required to provide a given SNR. The single sideband T_{sys} for CORAM operating at Ny-Ålesund is ~ 600 K. ~~Figure 2b shows the receiver noise temperature (Janssen, 1993) for CORAM measured at the exit of the cryocooler, with the cryocooler components at a typical temperature of 39 K. At 8.5 GHz, the receiver noise temperature is below 350 K.~~

~~The measurement time needed to produce a spectrum with a desired SNR is proportional to the square of the system noise temperature, which also includes contributions from the second downconversion, the atmospheric background and signal, and quasioptical spillover (Parrish et al., 1988, Janssen, 1993, Stanimirović et al., 2002).~~ ~~The single sideband system noise temperature of CORAM is ~ 600 K.~~

~~The measured signal is calibrated using two blackbody targets at known temperatures: a cold target in the cryocooler at ~ 70 K and a warm target at ~ 293 K. A path length modulator is part of the setup that directs the atmospheric signal to the feedhorn, in order to reduce the amplitude of any standing waves in the quasioptics. The FFTS is an Acqiris AC240 and has a bandwidth of 1 GHz with 16384 channels.~~The atmospheric measurements are all made with the same~~an~~ elevation angle ~~of 20°~~ and so the individually recorded spectra can be averaged together to reduce the SNR. The measurements used here have been spectrally averaged over approximately 1 hour, including time used to calibrate the signal. Finer time resolutions that still yield usefully high SNRs are possible. Since T_{sys}, as defined here, contains a component from the atmospheric background, the SNR of a given measurement will vary with the atmospheric conditions at the time, with a more opaque troposphere giving rise to a smaller SNR. An ad-hoc indication of "bad" weather conditions was found to be a measurement with a baseline temperature > 230 K, and these measurements were discarded.

2.2 CO profile retrieval ~~Inversion method~~

2.2.1 Defining the inversion problem

Schwarzchild's equation describes radiative transfer through a medium in local thermodynamic equilibrium. In the millimetre-wave region, at a given frequency, the measured intensity can be expressed in terms of brightness temperature, T_b, where

$$T_b = T_{b_0} e^{-\tau(l_0)} + \int_0^{l_0} T(l)\alpha(l)e^{-\tau(l)}dl, \quad (1)$$

with l denoting the path through the atmosphere from a point l_0 to the measurement point at $l = 0$. The initial intensity is T_{b_0}, the optical depth of the atmosphere is described by τ, and the absorption coefficient is defined as α. More details can be found in Janssen (1993) and references therein. T_b in Eq. (1), as a function of frequency, is generally the mathematical description of the calibrated atmospheric spectrum, the antenna temperature (T_a) from Sect. 2.1. For a total power radiometer such as CORAM, the calibrated antenna temperature is found using:

$$T_a = \left(\frac{V_{atm}-V_c}{V_h-V_c}\right)(T_h - T_c) + T_c, \quad (2)$$

where T_h and T_c are the temperatures of the hot and cold calibration targets (Sect. 2.1), and V_h and V_c are the measured voltages when observing the hot and cold targets, respectively. V_{atm} is the measured voltage when observing the atmosphere. The desired quantity, the VMR of a trace gas, is contained within the description of the absorption coefficient, α. Equation (1) must be inverted to retrieve this information. The form of Eq. (1) is that of a Fredholm integral of the second kind and is inherently sensitive to small perturbations (such as noise on a spectrum). To overcome this, the numerical inversion here is performed iteratively using a maximum a posteriori probability estimation.

2.2.2 Inversion method

Altitude profiles of CO VMR are retrieved from the measured spectra using an optimal estimation inversion technique (Rodgers, 2000). The method uses some a priori information of the state of the atmosphere to constrain the profile that is retrieved from the measured spectrum. The linear solution to the inversion problem can be expressed as $\hat{\mathbf{x}} = \mathbf{A}\mathbf{x} + (\mathbf{I} - \mathbf{A})\mathbf{x_a}$, where $\hat{\mathbf{x}}$ is the retrieved state vector (VMR profile), $\mathbf{x}$ is the true atmospheric state vector, $\mathbf{x_a}$ is the a priori state vector, and $\mathbf{I}$ is the identity matrix. $\mathbf{A}$ is the averaging kernel matrix, which describes ~~The averaging kernels describe~~ the sensitivity of a retrieved ~~CO VMR~~state ~~at a given altitude,~~ to the true state~~CO at other altitudes~~ (Rodgers, 2000). The sensitivity of the retrieved state at altitude i, to the true state at altitude j, is given by $\mathbf{A_{ij}} = \partial\hat{\mathbf{x}}_i / \partial\mathbf{x}_j$.

The inversions are performed with the Qpack2 package (Eriksson et al., 2005), which uses the Atmospheric Radiative Transfer Simulator (ARTS 2, Eriksson et al., 2011) to model the transfer of radiation through the earth's atmosphere. The a priori CO profile used in the inversion is the average of one winter (September through April) of output from the Whole Atmosphere Community Climate Model (WACCM4) (Garcia et al., 2007), provided by Douglas Kinnison at the National Centre for atmospheric research (NCAR). Model output for the grid point encompassing Ny-Ålesund is used. The output is

on a 132-layer pressure grid between approximately ground and 130 km altitude. A standard deviation of 100% at all altitudes was found to provide enough freedom for expected changes in CO VMR to be captured by the inversion, and to give enough regularisation of the solution. Oscillations in the CO profile, a sign of over-fitting to the measurement (Rodgers, 2000), were found in several profiles. The oscillations were large in these cases so the CO profiles were considered unphysical and rejected. CO emissions are attenuated by absorption due to water vapour in the atmosphere (mostly in the troposphere) and this is accounted for by including the water vapour continuum by Rosenkranz (1998) in the forward model and inversion. O_3 is also simultaneously retrieved with CO, as an O_3 spectral line is centred at ~~lies at~~ 231.28 GHz. The molecular oxygen (O_2) and nitrogen (N_2) continua (Rosenkranz, 1993), as well as nitric acid (HNO_3) spectral lines, are included in the inversion but are not retrieved and are considered model parameters. The spectroscopic line data used here are~~is~~ from the high resolution transmission molecular absorption database (HITRAN) 2008 catalogue (Rothmann et al., 2009). The a priori information for O_2 and O_3, and water vapour is from the same WACCM4 run as for CO, and the information for HNO_3 and N_2 are from the FASCOD (Fast Atmospheric Signature Code) subarctic winter scenario (Anderson et al., 1986).

The information for the altitude, pressure, and temperature in an inversion is constructed from European Centre for Medium-Range Weather Forecasting (ECMWF) profiles and from the NRLMSISE-00 empirical model of the atmosphere (MSIS from herein) (Picone et al., 2002). ECMWF information is available daily ~~four times per day~~at 6-hour intervals, beginning at midnight, and covers up to 0.01 hPa altitude, and above that the temperature profile information is from MSIS. The temperature data are~~is~~ smoothed around the point where the profiles are merged to avoid discontinuities.

An estimate of the measurement noise on a spectrum is made by fitting a second-order polynomial to a wing of the spectrum and calculating the standard deviation of the fit. Qpack2 provides the capability to fit a series of functions to the baseline of the measured spectra (a baseline fit) to account for errors in the baseline which are likely caused by standing waves in the instrument. The baseline fit is included in the optimal estimation and forms part of the overall fit to the measurement (inversion fit). All of the CORAM measured spectra were first inverted without a fit to the baseline and a periodogram of the residuals was evaluated to determine the periods of sinusoidal signatures in the baseline. Three primary sinusoids were found ~~to be present,~~ with respective estimated periods of 125, 62.5, and 41.67 MHz, and amplitudes of 0.2, 0.1, and 0.02 K. The periods of the sinewaves are large compared with the width of the CO spectral line, which has a typical full-width at half-maximum (FWHM) of ~0.7 MHz, and so are uniquely distinguishable from it. The broad wings of a CO spectral line are produced by CO molecules at altitudes below the retrievable altitude limit of CORAM (approximately 47 km, see Sect. 2.3). A first order polynomial is also included in the baseline fit to account for offsets. The zeroth- and first-order coefficients have estimated uncertainties of 1 K and 0.5 K respectively.

The altitude grid for the forward model is between the ground and 125 km, with approximately equally-spaced points. The retrieval grid is between approximately 2 and 124 km, and is a 62-layer subset of the forward model grid. CO VMRs are retrieved as a fraction of their a priori for numerical stability due to the strong gradients in atmospheric CO. The inversion method is nonlinear and uses a Marquardt–Levenberg iterative minimisation scheme (Marquardt, 1963).

2.3 CO profile characteristics

The CORAM CO data spans November 18th 2017 to January 18th 2018. The instrument required maintenance after the latteris date and was not in full operation for the remainder of the winter, unfortunately missing the SSW in February ☹. Nonetheless, the data shown here consists of 875 atmospheric profiles in that time, with time resolution of ~ 1 hr.

Figure 3 shows an example spectrum measured by CORAM on December 24th 2017, and the matching inversion fit and residual. The retrieved CO profile is also plotted in Fig. 3 alongside the a priori profile. The mean of the averaging kernels for the whole CO data set are shown in Fig. 4 alongside the average of the estimated altitude resolution of the CO profiles. ~~The averaging kernels describe the sensitivity of a retrieved CO VMR at a given altitude, to CO at other altitudes (Rodgers, 2000).~~ TThe estimated altitude resolution of the profiles is calculated here as the ~~full width at half maximum (~~FWHM~~)~~ of the averaging kernels. A common -way to estimate the altitude limits of a retrieved profile is to define the sum of the rows of the averaging kernels as the measurement response and assign a cut-off value. The measurement response can generally be thought of as a rough measure of the fraction of the retrieved state that comes from the data, rather than the a priori (Rodgers., 2000). As noted by Payne et al. (2009), this is only a rough measure, and the measurement response often exceeds 1 at some altitudes. The choice of the cut-off value is rather arbitrary but 0.8 is regularly used (e.g., Forkman~~n~~ et al., 2012; Straub et al., 2013, Schranz et al., 2018), and is also used here. With the above definitions, the CO profiles from CORAM during winter 2017/2018 have an average altitude range of approximately 47 – 87 km, with an average altitude resolution varying between approximately 12.5 and 28 km over that range. The retrieval range can change depending on the distribution of CO in the atmosphere (the lower limit can decrease in altitude when there are higher CO values at lower altitudes) and the value provided here is the mean range over the time span of the data.

The retrieval limits will vary from measurement to measurement and individual profiles should be considered in combination with the accompanying averaging kernels (see Fig. 4). The centres of the averaging kernels, when represented in VMR, are shifted down in altitude compared to a representation in relative units (Hoffmann et al., 2011). The lower limit of the retrieval here is defined by the SNR in the measurement and the upper limit is set by a transition from a pressure broadening regime to a doppler broadening one. The result of this change is that, above approximately 70 km in the VMR representation, the centres of the averaging kernels do not increase in altitude with their corresponding retrieval altitudes. The retrieved CO values above ~ 70 km altitude do contain information from the atmosphere that corresponds with the retrieval altitude, but the VMR representation of the profile should be considered with care. Hoffmann et al. (2011) provides a detailed discussion on the representation of data for ground-based CO measurements~~.~~. Hoffmann emphasises that the limited vertical resolution of the data must be taken into account for the use and interpretation of the data by considering each realisation of the averaging kernels, and so the a priori and averaging kernels form an essential part of the dataset.

2.4 CO profile error estimates

The error contributions to the CO profiles are calculated using OEM error definitions, which are defined in detail in Rodgers (2000). The estimates of the errors are found by perturbing the inputs to the inversion, using the following uncertainties. Error in the temperature profile is the same as that used in Hoffmann (2011): 10% above 100 km, 5% below 80 km, and linearly interpolated in between. An uncertainty of 1° is chosen for the pointing of the instrument to the sky, an overestimate of the motor (Faulhaber 3564K024B CS) uncertainty by an order of magnitude, to account for changes that may occur~~uncertainties~~ in the orientation of the instrument table. The uncertainty in the warm and cold calibration targets is 2 K, an overestimate that accounts for variations and drifts in the temperatures. The HITRAN 2008 catalogue is used for uncertainties in the CO line parameters: 1% for the line intensity, 2% for the air broadening parameter and 5% for the temperature dependence of the air broadening. The uncertainties related to self-broadening of CO are not considered due to the relatively low concentration of the gas (Ryan and Walker, 2015). The uncertainty in the line position is ignored because the frequency grid used in the inversion is~~can be~~ shifted to centre a measurement.

The error estimates, including the average of the error arising from statistical noise on the spectrum, are plotted in Fig. 5. The sum in quadrature of the error estimates is also plotted, as well as the a priori CO profile for the data set. The statistical noise on the spectrum and the uncertainty in the temperature profile are the biggest contributors to the total error profile, with the temperature error surpassing that of the spectrum noise at ~ 84 km, near the average upper retrieval altitude limit. As a fraction of the a priori profile, the total error estimate has a maximum at ~ 12% at ~ 48 km, near the average lower retrieval altitude limit, and there is also a peak of 11.5% near 70 km altitude. The uncertainty in the temperature profile begins to become more pronounced above 50 km altitude.

3 Comparison with Aura MLS

MLS is a radiometer aboard the Aura satellite. A description of the instrument is given in Waters et al. (2006). Version 4.2 of the MLS CO data (Schwartz et al., 2015) is used here and is described in Livesey et al. (2015). The atmospheric pressure range of the data is 215 - 0.0046 hPa. The precision of the CO VMR profile reaches a maximum (largest) value of 1.1 ppmv at the upper limit of the MLS CO retrieval altitude. The data have~~s~~ a positive bias of 20% in the middle atmosphere (larger VMRs), compared to the Atmospheric Chemistry Experiment – Fourier Transform Spectrometer (ACE-FTS) satellite instrument~~, of 20%~~ (Livesey et al., 2015). This bias is estimated from a study of V~~v~~ersion 2.2 of MLS CO data (Pumphrey et al., 2007), which showed a positive bias of 30 %. ~~with~~ S~~s~~ubsequent versions of MLS CO, including the version used here, show~~ing~~ a slight decrease in the CO VMR, bringing the values closer to those of ACE-FTS.

3.1 Colocated measurement comparison

MLS measurements are subset to within ±2° latitude and ±10° longitude of CORAM, calculated at 60 km altitude along the line of sight of CORAM (~ 156 km horizontally from the lab). The CO VMRs are expected to vary more in latitude than in longitude because the atmospheric composition generally varies more in the meridional direction compared to the zonal. A longitude space of ±5° was ~~also~~ tested but there were not significant changes to the results shown here and the number of coincident MLS measurements were halved. Above 0.001 hPa, MLS CO profiles have a ~~use a~~ constant VMR value. Because CORAM has some sensitivity to CO at these altitudes, the MLS profiles were instead linearly extrapolated in pressure space above 0.001 hPa. A more physically realistic profile shape is produced, an~~d~~ example of which can be seen in Fig. 4 of Ryan et al. (2017). To reduce the effect of atmospheric variability between individual measurement locations, the CORAM and MLS profiles are averaged by day to produce daily mean profiles. These MLS profiles were smoothed (Rodgers, 2000) with the averaging kernels of the corresponding CORAM profiles to account for the finer altitude resolution of MLS CO profiles: 6-7 km in the upper mesosphere and 3.5 to 5 km in the upper troposphere to the lower mesosphere (Livesey et al., 2015).

Figure 6 shows the mean CO profiles for CORAM and MLS over the time of measurement overlap ((~~mid~~ November 19th ~~to mid~~ January 18th), as well as the absolute and percentage (relative to the mean of the MLS and CORAM profiles) differences in the profiles. The correlation of the CO VMRs at each retrieval altitude is also plotted. The maximum absolute difference in the mean profiles is 2.5 ppmv at 86 km altitude, corresponding to an 11.3% difference. The percentage difference varies between ~ 7.4 % at the lowest retrieval altitude and 16.1% at 72 km, with MLS having a low bias in comparison to CORAM over the entire altitude range. This contrasts with the estimated high bias of MLS compared to ACE-FTS, mentioned above. The standard deviation of the differences in the profiles is largest (in percentage) at 58 km with a value of 14.4 %. The correlation of the CORAM and smoothed MLS CO profiles is greater than 0.80 at all retrieval altitudes, reaching a maximum of 0.92 at 47 km. After smoothing, the MLS and CORAM data are not truly independent, so the correlation of CORAM with the unsmoothed MLS data is also calculated and shows more variation over the retrievable altitude range, with a minimum of 0.59 and a maximum of 0.81. The statistics here show some similarities to the comparison of MLS CO and ground-based CO measurements from KIMRA (67.8° N), where MLS showed a low bias (peaking at ~ 0.65 ppmv) up to ~ 74 km, with a maximum relative bias of 22% at 60 km (Ryan et al., 2017). The correlation between KIMRA and MLS was slightly higher than that for CORAM and MLS, remaining greater than 0.90 up to 82 km ~~alttitude~~altitude.

Figure 7 shows the daily time series of the MLS and CORAM profiles at 48, 58, 68, 78, and 88 km. The largest differences in CO are found at higher altitudes (≥ 68 km) in November and the first days of December, after which the values become closer in VMR, indicating better agreement between the instruments. The reason for the larger difference over this time is unknown, but it is clear that these high values contribute to the bias between the instruments shown in Fig. 6. Despite the absolute differences, a similar variability in CO is captured by both instruments over the whole time series.

4 CORAM data and usage

Figure 8 shows the currently available CORAM CO data for winter 2017/2018 at 1 hr time resolution. The anomalously high values above ~ 70 km altitude are visible in November and first days of December. At lower altitudes over this time, there is still some downwelling of CO due to the residual mean circulation, before a levelling off in mid-December. ~~A general decrease in middle-atmospheric CO begins around December 22nd, leading to a local minimum in the first week of January.~~ Figure 8 also shows a 43-hour segment of the data beginning at 5 pm on December 31st 2017, to illustrate the advantage of continuous measurements. Below ~75 km altitude, there is apparent downwelling of CO for about the first 25 hours, peaking before VMR values start to decrease over the next 18 hours. There are two relatively strong increases in lower-altitude CO at approximately 2pm January 1st and 1am January 2nd, evident from the 2.3 ppmv contour line moving down from 60 to 50 km altitude. Over this same time, between 60 and 70 km, there is an oscillation in the 4.1 and 6 ppmv contour lines, with peaks occurring every 1-2 hours. The VMR values above approximately 75 km tend to show similar short-timescale variations but with opposite sign, i.e., a peak at a higher altitude corresponds with a trough at a lower altitude. This inverted pattern is observable over the whole 43-hour time period. Variations on these timescales cannot be directly observed by non-geostationary satellites, illustrating the unique capability of ground-based instruments.

These are broad descriptions of the data because one cannot fully characterise the variations in CO without the use of other data sources and model output. Variations on the timescales of an hour to weeks are visible in the data and require detailed study to elucidate the underlying dynamical processes, such as polar vortex shift, Rossby wave activity, SSW events, gravity wave perturbations (time scales of minutes to hours). Peridocities in trace gas data have previously been analysed using spectral decomposition techniques on ground-based measurements of water vapour and ozone (e.g., Struder et al., 2012, Hocke et al., 2013, Schranz et al., 2019) to identify waves with periods of days to weeks.

As mentioned in Sect. 2.3, the CORAM profiles should be used with consideration of the accompanying averaging kernels. Ground-based measurements have limited altitude resolution, often much coarser than the altitude grids onto which the data is retrieved. The representation of the data on a fine grid adds stability to the inversion (Eriksson, 1999) and can give rise to substantial smoothing error in the profiles (Rodgers, 2000). The smoothing error can be accounted for when comparing CORAM to instruments with higher resolution by convolving the data from the other instrument with the CORAM averaging kernels, as was done for MLS in Sect. 3. The error should be assessed if one is to use the CO profiles without considering the sensitivity distribution described by the averaging kernels. This is not a recommended use of the data and why the smoothing error is not assessed in Sect. 2.4. In other words, if one is to say something of a CORAM CO VMR at a given grid point, on must be aware that the VMR value at that grid point contains information from a range of altitudes, with a sensitivity governed by the associated averaging kernel.

CORAM profiles can be used independently to describe changes in CO over time, providing the averaging kernels do not significantly change over this time, which would change the measurement response. The measurement response for CORAM should not show significantly variation inside the retrievable altitude range but ~~In particular,~~ care should be taken at altitudes

near the edges of the retrieval range of the profiles, where the measurement response has a strong gradient and can change quickly when there are rapid changes in CO concentrations at those altitudes. CORAM is currently under maintenance due to a fault in the LO signal generator and is expected to be back in operation for the winter of 2019/2020 and beyond.

5 Conclusion and future work

This work presents a new ground-based radiometer, CORAM, that has been installed at the high-Arctic location of Ny-Ålesund, 78.9° N, for the measurement of middle-atmospheric CO. The instrument makes use of a high-frequency LNA, before the downconversion of the atmospheric signal, to achieve high SNRs at time resolutions on the order of an hour or less. CO profiles were retrieved from measurements in the Arctic winter of 2017/2018. ~~and~~ E~~e~~rror estimates show that the uncertainty in the temperature input for the inversions and the statistical noise on the spectrum are the largest contributions to the error budget, giving a maximum in the error profile of ~ 12 % of the a priori profile. The mean of the averaging kernel matrix for the CORAM dataset gives an average retrieval altitude range of 47-87 km with an average altitude resolution of 12.5 to 28 km over this range. Data at higher altitudes should be treated with care as the VMR representation of the averaging kernels do not peak at the corresponding retrieval grid points above ~70 km altitude. A comparison with MLS shows a negative bias (MLS - CORAM) at all altitudes, with a maximum of 16.1 % of the average profiles occurring at 72 km altitude. A comparison of the instruments' time series indicate abnormally high CO measured by CORAM above ~ 68 km in November 2017 that contributes to the observed bias, after which the MLS and CORAM values show improved agreement. Correlations between the instruments range from 0.80 to 0.92 over CORAMs retrievable altitude range for MLS data smoothed with the CORAM averaging kernels, and from 0.59 to 0.81 when using the unsmoothed MLS data. CO profiles above Ny-Ålesund with a 1 hr time resolution between November 19th 2017 and~~to~~ January 18th 2018 are currently available. Future work with CORAM will include: Integration of a newly manufactured local oscillator due to a failure of the original, and investigation of possible attenuation of the atmospheric signal by the laboratory foam window.

Data availability

CORAM Level 2 data, including averaging kernels and metadata, are available on request via N. Ryan (n_ryan@iup.physik.uni-bremen.de) and M. Palm (mathias@iup.physik.uni-bremen.de). A public data archive is planned for after CORAM resumes operation in the winter of 2019/2020. The Aura MLS v4.2 data are available from the Goddard Earth Sciences Data and Information Center at https://disc.gsfc.nasa.gov.

Author contribution

M. Palm and C. Hoffmann designed the project. C. Hoffmann, N. Ryan, and J. Goliasch designed and built CORAM. N. Ryan developed the inversion setups for CORAM and performed the comparisons. N. Ryan installed CORAM at Ny-Ålesund, and the instrument was maintained by M. Palm. J. Notholt provided valuable feedback on the project. N. Ryan prepared the manuscript with contributions from co-authors.

Acknowledgements

This work has been funded by the German Federal Ministry of Education and Research (BMBF) through the research project: Role Of the Middle atmosphere in Climate (ROMIC), sub-project: ROMICCO, project number: 01LG1214A, as well as by a grant from the Canadian Space Agency. We would like to express our gratitude to the MLS teams for making their CO product available. We would also like to thank the ECMWF and MSIS teams for making their products available, as well as the Qpack and ARTS communities for making their software available. We thank the AWIPEV staff for all of the help provided at Ny-Ålesund, particularly Benoit Laurent, who aided in the installation and maintenance of CORAM at Ny-Ålesund.

References

Allen, D., Stanford, J., Nakamura, N., López-Valverde, M., López-Puertas, M., Taylor, F., and Remedios, J.: Antarctic polar descent and planetary wave activity observed in ISAMS CO from April to July 1992. Geophys. Res. Lett., 27, 665–668, 2000.

Anderson, G. P., Clough, S. A., Kneizys, F. X., Chetwynd, J. H., and Shettle, E. P.: AFGL atmospheric constituent profiles (0–120 km), Tech. Rep. TR-86-0110, AFGL, 1986.

Bailey, S. M., Thurairajah, B., Randall, C. E., Holt, L., Siskind, D. E., Harvey, V. L., Venkataramani, K., Hervig, M. E., Rong, P., and Russell III, J. M.: A multi tracer analysis of thermo- sphere to stratosphere descent triggered by the 2013 Stratospheric Sudden Warming, Geophys. Res. Lett., 41, 5216–5222, doi:10.1002/2014GL059860, 2014.

Andrews, D., Holton, J., and Leovy, C.: Middle Atmosphere Dynamics, Academic Press, 489 pp., 1987.

Di Biagio, C., Muscari, G., di Sarra, A., de Zafra, R. L., Eriksen, P., Fiocco, G., Fiorucci, I., and Fuà, D.: Evolution of temperature, O3, CO, and N2O profiles during the exceptional 2009 Arctic major stratospheric warming observed by lidar and mm-wave spectroscopy at Thule (76.5 N, 68.8 W), Greenland, J. Geophys. Res., 115, D24315, doi:10.1029/2010JD014070, 2010.

Brasseur, G. and Solomon, S.: Aeronomy of the Middle Atmosphere: Chemistry and Physics of the Stratosphere and Mesosphere, Springer, 644 pp., 2005.

Brinksma, E. J., Meijer, Y. J., McDermid, I. S., Cageao, R. P., Bergwerff, J. B., Swart, D. P. J., Ubachs, W., Matthews, W. A., Hogervorst, W., and Hovenier, J. W.: First lidar observations of mesospheric hydroxyl, Geophys. Res. Lett., 25, 51-54, 1998.

Chane Ming, F., Vignelles, D., Jegou, F., Berthet, G., Renard, J.-B., Gheusi, F., and Kuleshov, Y.: Gravity-wave effects on tracer gases and stratospheric aerosol concentrations during the 2013 ChArMEx campaign, Atmos. Chem. Phys., 16, 8023-8042, https://doi.org/10.5194/acp-16-8023-2016, 2016.

Damiani, A., Storini, M., Santee, M. L., and Wang, S.: Variability of the nighttime OH layer and mesospheric ozone at high latitudes during northern winter: influence of meteorology, Atmos. Chem. Phys., 10, 10291-10303, doi:10.5194/acp-10-10291-2010, 2010.

Damiani, A., Funke, B., Puertas, M. L., Gardini, A., Santee, M. L., Froideveaux, L., and Cordero, R. R.: Changes in the composition of the northern polar upper stratosphere in February 2009 after a sudden stratospheric warming, J. Geophys. Res.-Atmos., 119, 11429–11444, doi:10.1002/2014JD021698, 2014.

Eckermann, S. D., Gibson-Wilde, D. E., and Bacmeister, J. T.: Gravity Wave Perturbations of Minor Constituents: A Parcel Advection Methodology, J. Atmos. Sci., 55, 3521–3539, 1998.

Eriksson P.: Microwave radiometric observations of the middle atmosphere: simulations and inversions. Ph.D. thesis, Chalmers University of Technology, 1999.

Eriksson, P., Jimenez, C., and Buehler, S. A.: Qpack, a general tool for instrument simulation and retrieval work, JQSRT, 91(1), 47-64, 2005.

Eriksson, P., Buehler, S. A., Davis, C. P., Emde, C., and Lemke, O.: ARTS, the atmospheric radiative transfer simulator, Version 2. JQSRT, 112, 1551-1558, 2011.

Fernandez, S., Murk, A., and Kämpfer, N.: GROMOS-C, a novel ground-based microwave radiometer for ozone measurement campaigns, Atmos. Meas. Tech., 8, 2649-2662, https://doi.org/10.5194/amt-8-2649-2015, 2015.

Forkman, P., Eriksson, P., and Murtagh, D.: Observing the vertical branch of the mesospheric circulation at lat N60˚ using ground based measurements of CO and H2O, J. Geophys. Res., 110, 107, doi:10.1029/2004JD004916, 2005.

Forkman, P., Christensen, O. M., Eriksson, P., Urban, J., and Funke, B.: Six years of mesospheric CO estimated from ground-based frequency-switched microwave radiometry at 57° N compared with satellite instruments, Atmos. Meas. Tech., 5, 2827–2841, doi:10.5194/amt-5-2827-2012, 2012.

Fritts, D. C., and Alexander, M., J.: Gravity wave dynamics and effects in the middle atmosphere, Rev. Geophys., 41, 1003, doi:10.1029/2001RG000106, 2003.

~~Janssen M.A.: Atmospheric remote sensing by microwave radiometry, Wiley, New York, 37-90, 1993.~~

Garcia, R. R. and Solomon, S.: A Numerical Model of the Zonally Averaged Dynamical and Chemical Structure of the Middle Atmosphere, J. Geophys. Res., 88, 1379–1400, doi:10.1029/JC088iC02p01379, 1983.

Garcia, R., Marsh, D., Kinnison, D., Boville, B., and Sassi, F.: Simulation of secular trends in the middle atmosphere, 1950-2003, J. Geophys. Res., 112, D09301, doi:10.1029/2006JD007485, 2007.

Garcia, R. R., López-Puertas M., Funke D., Marsh D. R., Kinnison D. E., Smith A. K., and González-Galindo F.: On the distribution of CO2 and CO in the mesosphere and lower thermosphere, J. Geophys. Res., 119, 5700–5718, doi:10.1002/2013JD021208, 2014.

Goldsmith, P. F.: Quasioptical Systems: Gaussian Beam Quasioptical Propagation and Applications, IEEE, New York, 1988.

Hocke, K., Kämpfer, N, Feist, D. G., Calisesi, Y., Jiang, J. H., and Chabrillat, S.: Temporal variance of lower mesospheric ozone over Switzerland during winter 2000/2001, Geophys. Res. Lett., 33, L09801, doi:10.1029/2005GL025496, 2006.

Hoffmann, C. G., Raffalski, U., Palm, M., Funke, B., Golchert, S. H. W., Hochschild, G., and Notholt, J.: Observation of stratomesospheric CO above Kiruna with ground-based microwave radiometry – retrieval and satellite comparison, Atmos. Meas. Tech., 4, 2389–2408, doi:10.5194/amt-4-2389-2011, 2011.

Hoffmann, C. G.: Application of CO as a tracer for dynamics in the polar winter middle atmosphere, Ph.D. thesis, Institut für Umweltphysik, Universität Bremen, Germany, 142 pp., 2012.

Janssen M.A.: Atmospheric remote sensing by microwave radiometry, Wiley, New York, 37-90, 1993.

Kasai, Y. J., Koshiro, T., Endo, M., Jones, N. B., and Murayama, Y.: Ground-based measurement of strato-mesospheric CO by a FTIR spectrometer over Poker Flat, Alaska. Adv Space Res, 35, 2024-2030, 2005.

Kindlmann, G., Reinhard, E., and Creem, S.: Face-based lightness Matching for Perceptual Colormap Generation, IEEE Proceedings of the conference on Visualization 2002, available at: www.cs.utah.edu/~gk/papers/vis02/FaceLumin.pdf, 2002.

Lee, J. N., Wu, D. L., Manney, G. L., Schwartz, M. J., Lambert, A., Livesey, N. J., Minschwaner, K. R., Pumphrey, H. C., and Read, W. G.: Aura Microwave Limb Sounder observations of the polar middle atmosphere: Dynamics and transport of CO and H2O, J. Geophys. Res., 116, D05110, doi:10.1029/2010JD014608, 2011.

Livesey, N. J., Read, W. G., Wagner, P. A., Froidevaux, L., Lambert, A., Manney, G. L., Millán Valle, L. F., Pumphrey, H. C., Santee, M. L., Schwartz, M. J., Wang, S., Fuller, R. A., Jarnot, R. F., Knosp, B. W., and Martinez, E.: Version 4.2x Level 2 data quality and description document, Tech. rep., Jet Propulsion Laboratory, 2015.

Manney, G. L., Schwartz, M. J., Krüger, K., Santee, M. L., Pawson, S., Lee, J. N., Daffer, W. H., Fuller, R. A., and Livesey, N. J.: Aura Microwave Limb Sounder observations of dynamics and transport during the record-breaking 2009 Arctic stratospheric major warming, Geophys. Res. Lett., 36, L12815, doi:10.1029/2009GL038586, 2009.

Manney, G. L., Lawrence, Z. D., Santee, M. L., Read, W. G., Livesey, N. J., Lambert, A., Froidevaux, L., Pumphrey, H. C., and Schwartz, M. J.: A minor sudden stratospheric warming with a major impact: Transport and polar processing in the 2014/2015 Arctic winter, Geophys. Res. Lett., 42, 7808–7816, doi:10.1002/2015GL065864, 2015.

Marquardt, D.: An algorithm for least squares estimation on nonlinear parameters, J. Soc. Ind. Appl. Math., 11, 431–41, 1963.

McLandress, C., Scinocca, J. F., Shepherd, T. G., Reader, M. C., and Manney, G. L.: Dynamical Control of the Mesosphere by Orographic and Nonorographic Gravity Wave Drag during the Extended Northern Winters of 2006 and 2009, J. Atmos. Sci., 70, 2152–2169, doi:10.1175/JAS-D-12-0297.1, 2013.

Nassar, R., Bernath, P. F., Boone, C. D., Manney, G. L., McLeod, S. D., Rinsland, C. P., Skelton, R., and Walker, K. A.: ACE-FTS measurements across the edge of the winter 2004 Arctic vortex, Geophys. Res. Lett., 32, L15S05, doi:10.1029/2005GL022671, 2005.

Noguchi, K., Imamura, T., Oyama, K. -I., and- Bodeker, G. E: A global statistical study on the origin of small-scale ozone vertical structures in the lower stratosphere, J. Geophys. Res., 111, D23105, doi:10.1029/2006JD007232, 2006.

Parrish, A., de Zafra, R. L., Solomon, P. M., and Barrett, J. W.: A ground-based technique for millimeter wave spectroscopic observations of stratospheric trace constituents, Radio Sci., 23, 106–118, 1988.

Picone, J.M., Hedin, A.E., Drob, D.P., and Aikin, A.C.: NRL-MSISE-00 Empirical Model of the Atmosphere: Statistical Comparisons and Scientific Issues, J. Geophys. Res., doi:10.1029/2002JA009430, 2002.

Pumphrey, H. C., Filipiak, M. J., Livesey, N. J., Schwartz, M. J., Boone, C., Walker, K. A., Bernath, P., Ricaud, P., Barret, B., Clerbaux, C., Jarnot, R. F., Manney, G. L., and Waters, J. W.: Validation of middle-atmosphere carbon monoxide retrievals from MLS on Aura, J. Geophys. Res., 112, D24S38, doi:10.1029/2007JD008723, 2007.

Raffalski, U., Hochschild, G., Kopp, G., and Urban, J.: Evolution of stratospheric ozone during winter 2002/2003 as observed by a ground-based millimetre wave radiometer at Kiruna, Sweden, Atmos. Chem. Phys., 5, 1399–1407, doi:10.5194/acp-5-1399-2005, 2005.

Rodgers, C. D. and Connor, B. J.: Intercomparison of remote sounding instruments, J. Geophys. Res., 108, 4116, doi:10.1029/2002JD002299, 2003.

Rodgers, C. D.: Inverse methods for atmospheric remote sounding: Theory and practice. Vol 2. Series on atmospheric and ocean physics. Singapore: World Scientific, 2000.

Rosenkranz, P.W.:Water vapor microwave continuum absorption: A comparison of measurements and models, Radio Science, 33, 919–928, 1998.

Rosenkranz, P.W.: Absorption of microwaves by atmospheric gases, in: Janssen M.A.: Atmospheric remote sensing by microwave radiometry, Wiley, New York, 37-90, 1993.

Rothman, L. S., Gordon, I. E., Barbe, A., Chris Benner, D., Bernath, P. F., Birk, M., Boudon, V., Brown, L. R., Campargue, A., Champion, J. –P., Chance, K., Couderti, L. H., Dana, V., Devi, V. M., Fally, S.,Flaud, J. –M., Gamache, R. R., Goldman, A., Jacquemart, D., Kleiner, I., Lacome, N., Lafferty, W. J., Mandin, J. –Y., Massie, S. T., Mikhailenko, S. N., Miller, C. E., Moazzen-Ahmadi, N., Naumenko, O. V., Nikitin, A. V., Orphal, J., Perevalov, V. I., Perrin, A., Predoi-Cross, A., Rinsland, C. P., Rotger, M., Simeckova, M., Smith M. A. H., Sung K., Tashkun, S. A., Tennyson, J., Toth, R. A., Vandaele, A. C., and Vander Auwera, J.: The HITRAN 2008 molecular spectroscopic database, J. Quant. Spec. Rad. Trans., 110(9-10), 533-572, 2009.

Ryan, N. J., and Walker, K. A.: The effect of spectroscopic parameter inaccuracies on ground-based millimeter wave remote sensing of the atmosphere. JQSRT, 161, 50-59, doi:10.1016/j.jqsrt.2015.03.012, 2015.

Ryan, N. J., Palm, M., Raffalski, U., Larsson, R., Manney, G., Millán, L., and Notholt, J.: Strato-mesospheric carbon monoxide profiles above Kiruna, Sweden (67.8 ° N, 20.4 ° E), since 2008, Earth Syst. Sci. Data, 9, 77-89, doi:10.5194/essd-9-77-2017, 2017.

Ryan, N. J., Kinnison, D. E., Garcia, R. R., Hoffmann, C. G., Palm, M., Raffalski, U., and Notholt, J.: Assessing the ability to derive rates of polar middle-atmospheric descent using trace gas measurements from remote sensors, Atmos. Chem. Phys., 18, 1457-1474, https://doi.org/10.5194/acp-18-1457-2018, 2018.

Schranz, F., Fernandez, S., Kämpfer, N., and Palm, M.: Diurnal variation in middle-atmospheric ozone observed by ground-based microwave radiometry at Ny-Ålesund over 1 year, Atmos. Chem. Phys., 18, 4113-4130, https://doi.org/10.5194/acp-18-4113-2018, 2018.

Schranz, F., Tschanz, B., Rüfenacht, R., Hocke, K., Palm, M., and Kämpfer, N.: Investigation of Arctic middle-atmospheric dynamics using 3 years of H2O and O3 measurements from microwave radiometers at Ny-Ålesund, Atmos. Chem. Phys. Discuss., https://doi.org/10.5194/acp-2018-1299, in review, 2019.

Schwartz, M., Pumphrey, H., Livesey, N. and Read, W.: MLS/Aura Level 2 Carbon Monoxide (CO) Mixing Ratio V004, version 004, Greenbelt, MD, USA, Goddard Earth Sciences Data and Information Services Center (GES DISC), Accessed June 2018 at 10.5067/AURA/MLS/DATA2005.

Smith, A. K., Garcia, R. R., Marsh, D. R., and Richter J. H.: WACCM simulations of the mean circulation and trace species transport in the winter mesosphere, J. Geophys. Res., 116, D20115, doi:10.1029/2011JD016083, 2011.

Solomon, S., Garcia, R. R., Olivero, J. G., Bevilacqua, R. M., Schwarzt, P. R., Clancy, R. T., and Muhleman, D. O.: Photochemistry and Transport of Carbon Monoxide in the Middle Atmosphere, J. Atmos. Sci., 42(10), 1072-1083, 1985.

Stanimirovic, S., Altschuler, D., Goldsmith, P., Salter, C.:Single-Dish Radio Astronomy: Techniques and Applications, ASP Conf. Ser., vol. 278, 2002.

Straub, C., Murk, A., and Kämpfer, N.: MIAWARA-C, a new ground based water vapor radiometer for measurement campaigns, Atmos. Meas. Tech., 3, 1271-1285, https://doi.org/10.5194/amt-3-1271-2010, 2010.

Straub, C., Tschanz, B., Hocke, K., Kämpfer, N., and Smith, A. K.: Transport of mesospheric H2O during and after the stratospheric sudden warming of January 2010: observation and simulation, Atmos. Chem. Phys., 12, 5413–5427, doi:10.5194/acp-12-54132012, 2012.

Straub, C., Espy, P., Hibbins, R. E., and Newnham, D. A.: Mesospheric CO above Troll station, Antarctica observed by a ground based microwave radiometer. Earth Syst. Sci. Data, 5, 199–208, doi:10.5194/essd-5-199-2013, 2013.

Studer, S., Hocke, K., Schanz, A., Schmidt, H., and Kämpfer, N.: A climatology of the diurnal variations in stratospheric and mesospheric ozone over Bern, Switzerland, Atmos. Chem. Phys., 14, 5905-5919, https://doi.org/10.5194/acp-14-5905-2014, 2014.

Velazco, V., Wood, S. W., Sinnhuber, M., Kramer, I., Jones, N. B., Kasai, Y., Notholt, J., Warneke, T., Blumenstock, T., Hase, F., Murcray, F. J., and Schrems, O.: Annual variation of strato-mesospheric carbon monoxide measured by ground-based Fourier transform infrared spectrometry. Atmos. Chem. Phys., 7, 1305-1312, 2007.

Vowinkel, B.: Passiv Mikrowellenradiometrie, Vieweg+Teubner Verlag, Weisbaden, https://doi.org/10.1007/978-3-322-86042-2, 1988.

Waters, J., Froidevaux, L., Harwood, R., Jarno, R., Pickett, H., Read, W., Siegel, P., Cofield, R., Filipiak, M., Flower, D., Holden, J., Lau, G., Livesey, N., Manney, G., Pumphrey, H., Santee, M., Wu, D., Cuddy, D., Lay, R., Loo, M., Perun, V., Schwartz, M., Stek, P., Thurstans, R., Boyles, M., Chandra, S., Chavez, M., Chen, G.-S., Chudasama, B., Dodge, R., Fuller, R., Girard, M., Jiang, J., Jiang, Y., Knosp, B., LaBelle, R., Lam, J., Lee, K., Miller, D., Oswald, J., Patel, N., Pukala, D., Quintero, O., Scaff, D., Snyder, W., Tope, M., Wagner, P., and Walch, M.: The Earth Observing System Microwave Limb Sounder (EOSMLS) on the Aura satellite, IEEE T. Geosci. Remote, 44, 1075–1092, 2006.

Zhu, X., and J. R. Holton, J., R.: Mean fields induced by local gravity-wave forcing in the middle atmosphere, J. Atmos. Sci., 44, 620–630, 1987.

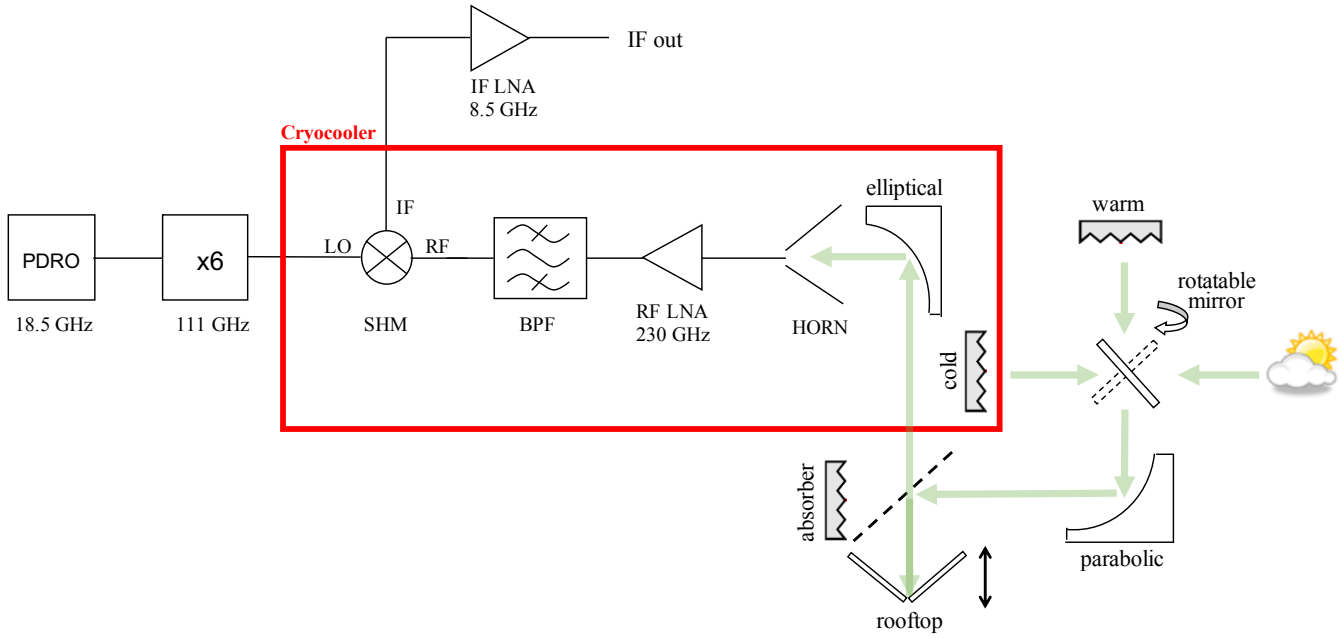

Figure 1: Schematic of the CORAM receiver and simplified version of the quasiopticsreceiver. AThe rotatable mirror selects a signal from either the atmosphere, warm target, or cold target. The signal is directed by a parabolic mirror to a path length modulator that comprises a polarising wire grid, an absorber, and an oscillating rooftop mirror. The signal passes through a window in the cryocooler where it is directed to the receiver with an elliptical mirror.atmospheric signal The signal enters the passes through the quasioptical system (not shown) and a window in the cryocooler before reaching (in order) a corrugated feed horn and encounters, a 230 GHz the RF LNA, a waveguide filter (BPF), and a sub-harmonic mixer (SHM). At the SHM, where the signal is downconverted to an intermediate frequency (IF) of 8.5 GHz. The IF signal signal exits the cryocooler and passes through a room temperature LNA. The atmospheric signalRF (atmospheric) signal is mixed at the SHM with a local oscillator (LO) signal, which is an 18.5 GHz signal from a phase-locked dielectric resonator oscillator (PDRO) that is passed through a xX6 frequency multiplier, to provide 111 GHz at the SHM. The IF out signal will be further downconverted to 0.5 GHz before being analysed by the Fast Fourier Transform Spectrometer (not shown here). Further details on quasioptical components can be found in Goldsmith (1998).

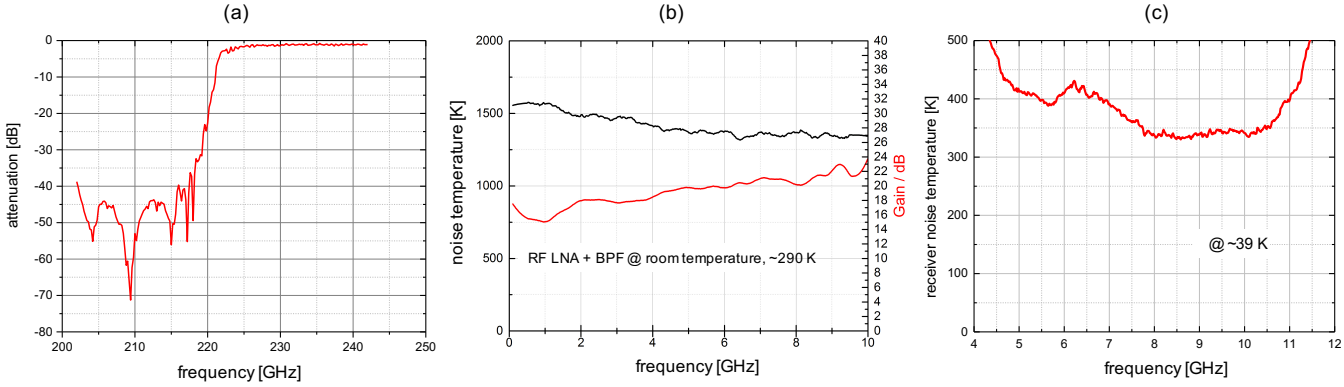

Figure 2: (a) The frequency response of the waveguide filter (BPF in Fig. 1) used in CORAM to supress the unwanted sideband signal at 213.5 GHz. ~~The frequency response of the waveguide filter (BPF in Fig. 1) in used in CORAM to supress the unwanted sideband signal at 213.5 GHz.~~ **(b)** The noise temperature and gain of the RF LNA + BPF (Fig. 1) at room temperature. ~~The receiver noise temperature for CORAM after downconversion to 8.5 GHz. This measurement is made after the first room temperature LNA (Fig. 1) and before the second downconversion to 1.5 GHz. The cryocooler components are at 39 K. The single sideband system noise temperature for CORAM is ~ 600 K (Sect. 2.1).~~(c) The noise temperature for CORAM after downconversion to 8.5 GHz. This measurement is made after the first IF LNA (Fig. 1) and before the second downconversion to 0.5 GHz. The cryocooler components are at 39 K. The single sideband system temperature for CORAM is ~ 600 K (Sect. 2.1).

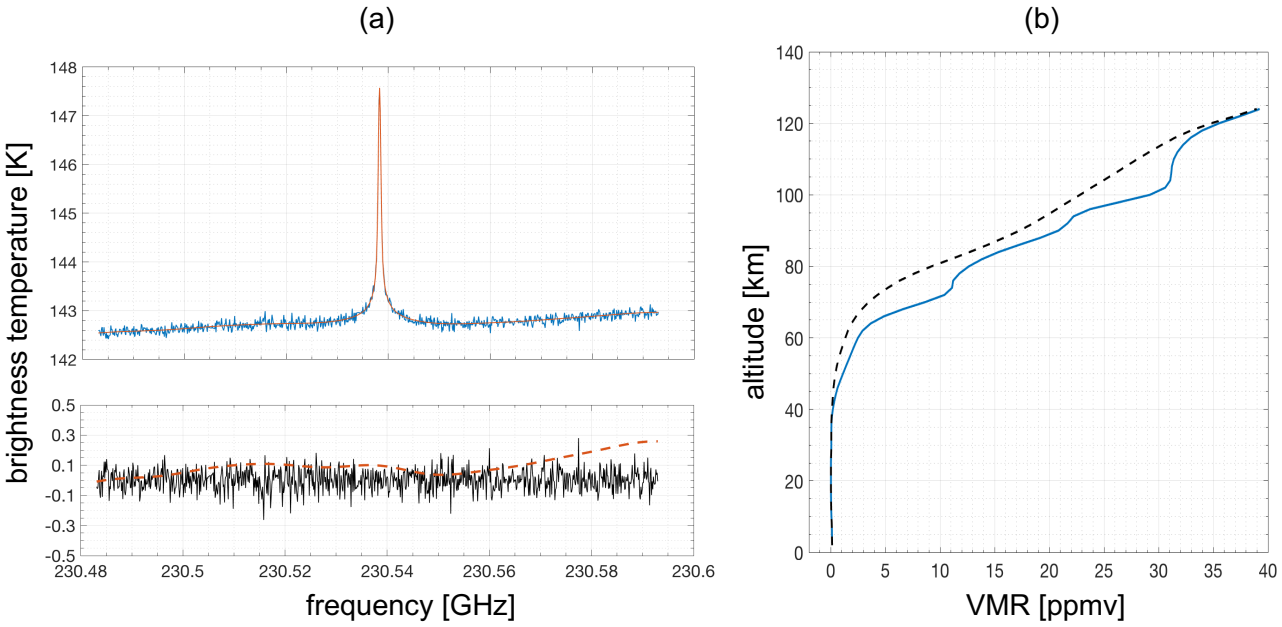

Figure 3: (a) Upper: an example spectrum measured by CORAM on Dec 24th 2017 between 20:04 and 21:03 UTC. The inversion fit to the measurement is shown (smoother red line). Lower: the residual of the measurement and the inversion fit (solid black line). The dashed red line shows the baseline fit for the inversion, which is part of the inversion fit shown in the upper panel (Sect. 2.2.2). (b) The CO profile retrieved from the measurement (solid blue) and the a priori profile that is used as input to the inversion (dashed black).

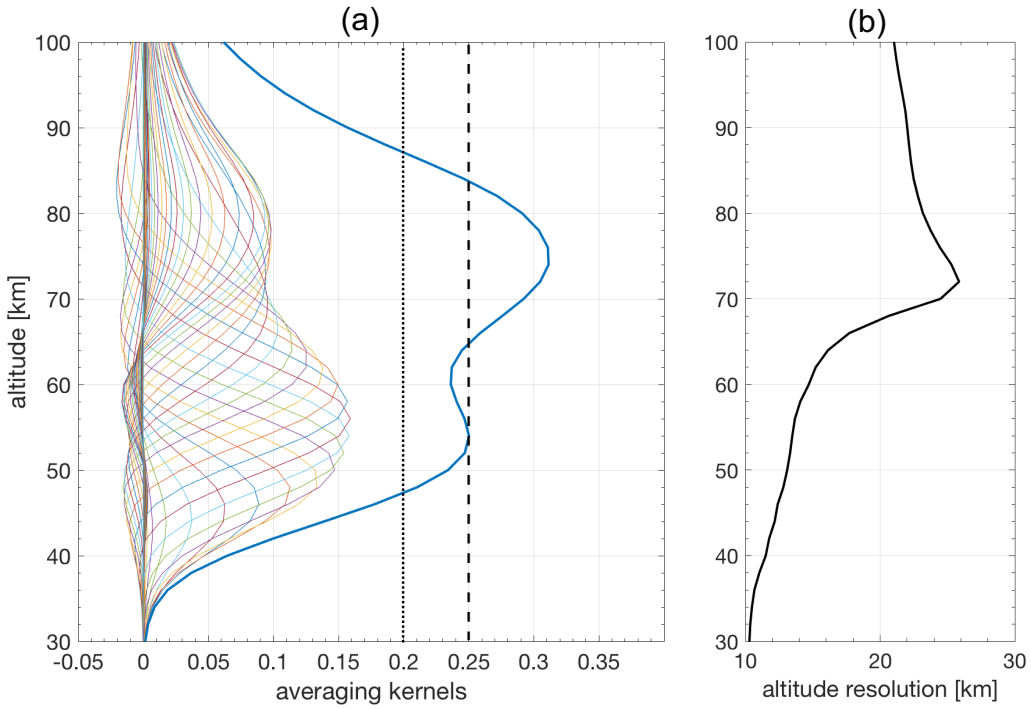

Figure 4: The mean averaging kernels for the CORAM inversions. The measurement response (sum of the rows of the averaging kernels) divided by 4 is shown in thick solid blue. The dashed black line and the dotted black line indicate a measurement response of 1.0 and 0.8, respectively. (b) The mean altitude resolution of the CORAM CO profiles, calculated from the FWHM of the averaging kernels.

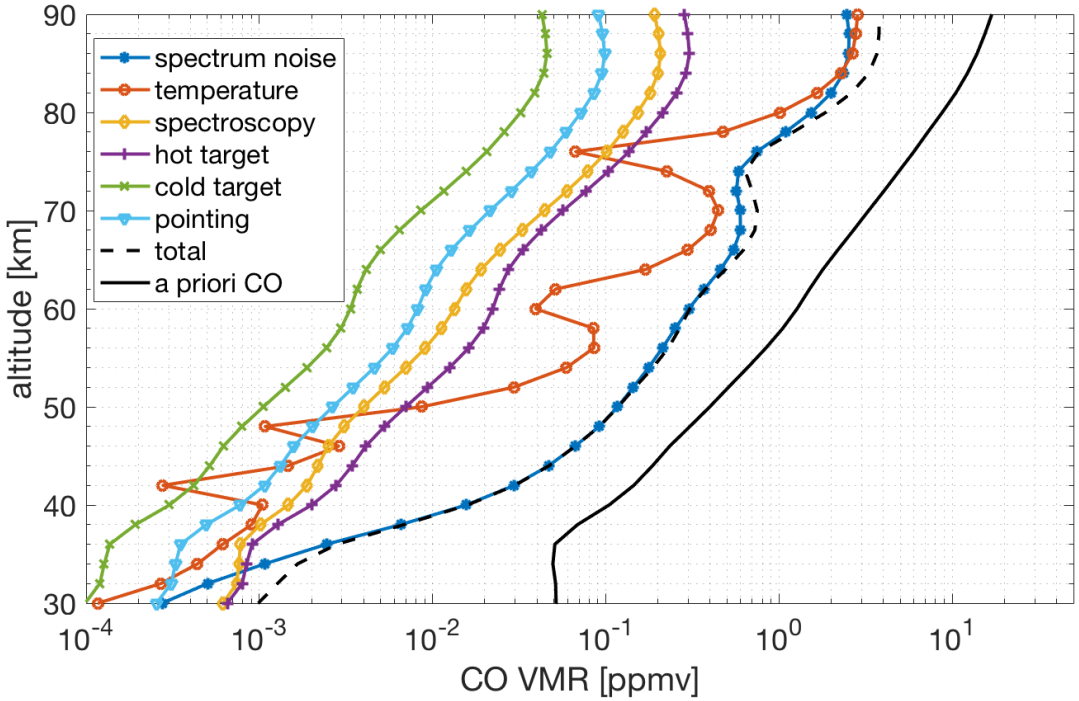

Figure 5: The estimated error contributions to the CORAM CO profiles. The spectrum noise is calculated as an average of the noise on all CORAM measurements, and the other estimates are calculated through perturbations about the a priori CO profile (Sect. 2.4).

5

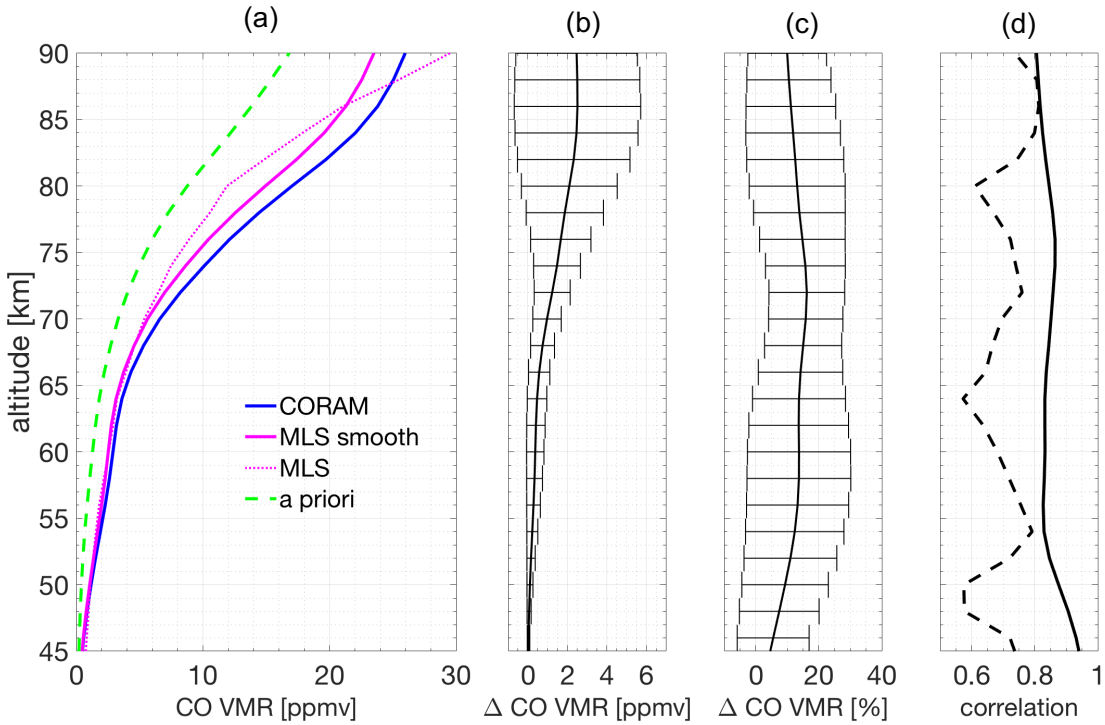

Figure 6: (a) The mean of the daily CORAM and MLS CO profiles above Ny-Ålesund. The mean of the unsmoothed MLS profiles is also shown as well as the a prioiri profile used for the CORAM inversions. (b) The absolute difference of the mean CORAM and smoothed MLS profiles, with the standard deviation of the differences as the whiskers on the line. (c) The same as for (b) but with the difference as a percentage of the mean CORAM and MLS profiles. (d) The correlation coefficients of the CORAM and smoothed MLS data (solid) and unsmoothed MLS data (dashed).

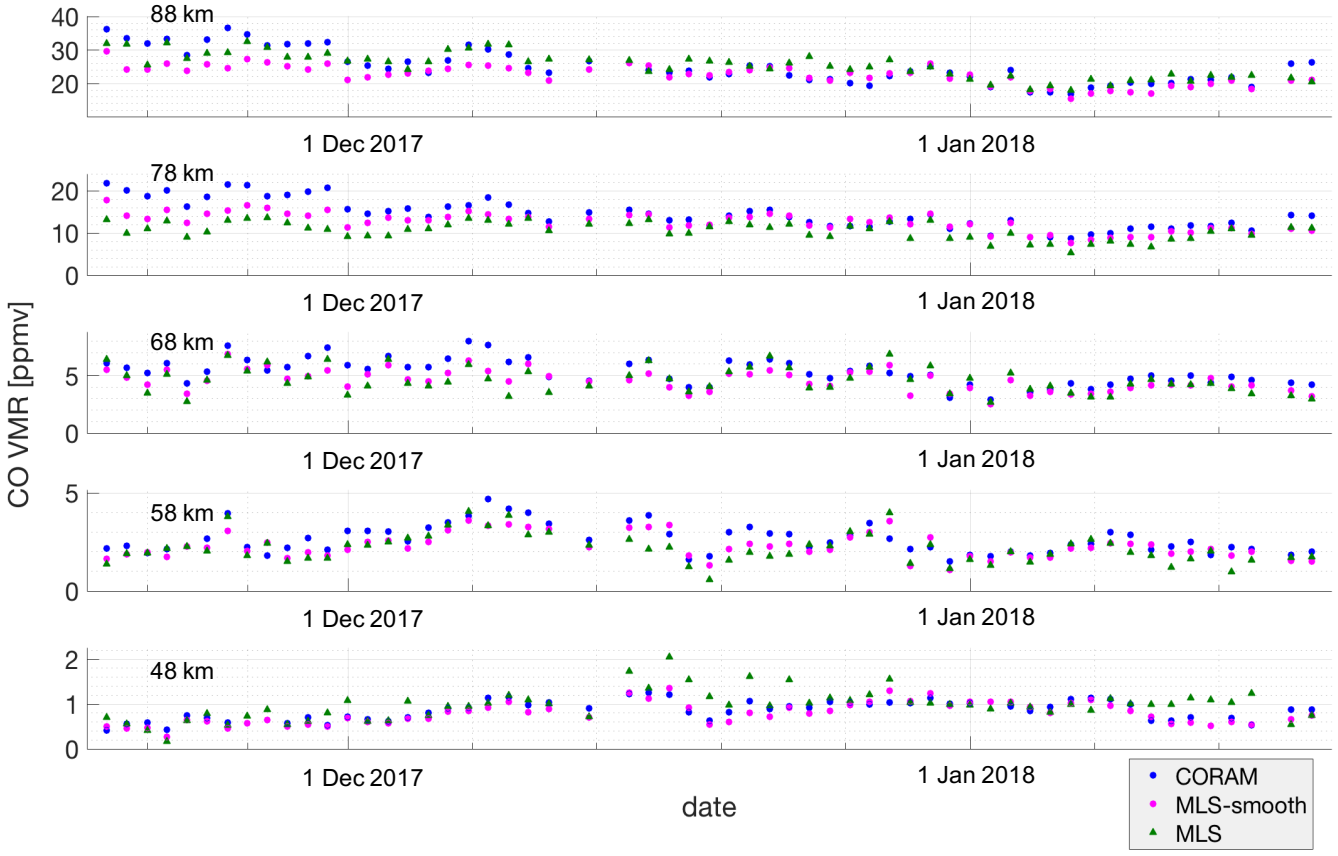

Figure 7: Time series of the daily CORAM and MLS CO ~~profiles~~VMR values at altitudes of 48, 58, 68, 78, and 88 km.

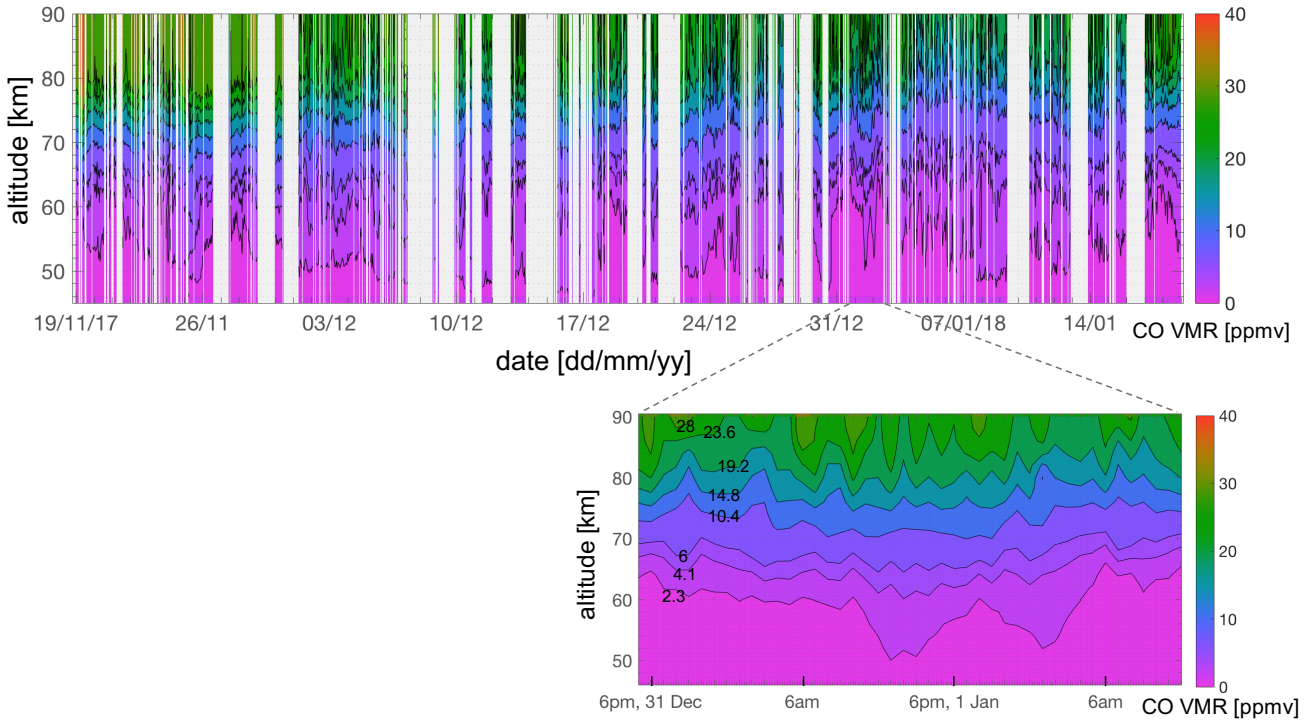

Figure 8: CORAM CO profiles at 1 hr resolution from mid-November 2017 to mid-January 2018. Blank areas are gaps in the data record. The zoomed-in plot shows measurements over a 42-hour period beginning at 6pm on December 31st 2017. ~~The contours are non-uniformly spaced between 0.4 and 28 ppmv, and filled to ease readability.~~ The Isoluminant colour map from Kindlmann et al. (2002) is used. Contour values are [0.4, 2.3, 4.1, 6.0, 10.4, 14.8, 19.2, 23.6, 28.0], chosen and filled for readability. Gaps in the data record correspond to periods of non-operation or bad measurement data.